Applied Catalysis B: Environmental 342 (2024) 123360

Contents lists available at ScienceDirect

Applied Catalysis B: Environmental

journal homepage: www.elsevier.com/locate/apcatb

Fe-MOR and Fe-FER as catalysts for abatement of N_2O with CH_4: *in situ* UV–vis DRS and *operando* FTIR study

Maria Cristina Campa [a,*], Daniela Pietrogiacomi [b], Carlotta Catracchia [b], Simone Morpurgo [b], Joanna Olszowka [c], Kinga Mlekodaj [c], Mariia Lemishka [c,d], Jiri Dedecek [c], Agnieszka Kornas [c], Edyta Tabor [c,*]

[a] CNR-Institute for Nanostructured Materials (ISMN), c/o Department of Chemistry, "Sapienza" University of Rome, P.le Aldo Moro 5, 00185 Rome, Italy
[b] Department of Chemistry, "Sapienza" University of Rome, P.le Aldo Moro 5, 00185 Rome, Italy
[c] J. Heyrovský Institute of Physical Chemistry of the CAS v. v. i., Dolejškova 2155/3, 182 23 Prague, Czech Republic
[d] Faculty of Chemical Technology, University of Pardubice, Studentská 95, 532 10 Pardubice, Czech Republic

ARTICLE INFO

Keywords:
Zeolite
Al-distribution
Fe-MOR
Fe-FER
N_2O abatement with CH_4
Operando FTIR

ABSTRACT

The catalytic reduction of N_2O with CH_4 in absence or in presence of O_2 (CR_{N2O} or SCR_{N2O}) and H_2O (hydrothermal conditions) was studied on Fe-MOR and Fe-FER catalysts with similar Al distribution and iron-loading. In N_2O decomposition and SCR_{N2O} Fe-FER catalysts were more active than Fe-MOR, whereas in CR_{N2O} the catalysts exhibited similar activity. *In situ* FTIR and UV–vis spectroscopies of thermally activated catalysts revealed that Fe(II) species are better stabilized in FER than in MOR topology. In the presence of CH_4, Fe(III)-oxo species were reduced to Fe(II) in both zeolites and became active sites for the CR_{N2O} process. In SCR_{N2O} the presence of O_2 decreased the activity of Fe-MOR due to a partial re-oxidation of the active sites. The addition of H_2O to the feed caused a poor and reversible deactivation. *Operando* FTIR experiments provided insights into the reaction pathways and suggested formaldehyde and formate surface species as intermediates.

1. Introduction

Nitrous oxide (N_2O) with its high global warming potential (ca. 310 times higher than CO_2) and long lifetime in the atmosphere (114 years) significantly contributes to the greenhouse effect and ozone layer depletion [1]. Among the main anthropogenic sources of N_2O, production of nitric and adipic acids, fossil-fuel combustion processes (power plants), and three-way catalyst converters are included [1]. The decrease in N_2O emission, controlled through EU legislation [2], can be accomplished by the employment of heterogeneous catalysts, as metal-lozeolites (zeolites with embedded transition metal ion species), which represent a very promising group of catalysts for N_2O abatement *via* decomposition and reduction [3–6]. In particular, Fe-zeolites exhibit high catalytic performance and find application in nitric acid plants where EnviNOx® process [7], besides NO, abates N_2O by decomposition or reduction with hydrocarbons. The unique catalytic properties of Fe-zeolites are strongly related to the nature of iron species embedded in the aluminosilicate matrix. To develop a new generation of highly active and selective catalysts able to lead the chemical industry towards sustainability, it is necessary to clarify the structure and performance of active sites at the atomic level.

Among Si-rich zeolites, the organization of Al atoms in the zeolite matrix is one of the features that significantly influence the stabilization of particular iron species, and therefore the catalytic performance. Al atoms introduce a negative charge in the zeolite lattice and stabilize divalent cations if present as Al pairs (two Al atoms in the same zeolite ring), or trivalent-oxo monovalent cationic species if present as single Al atoms [8,9]. At low Fe-loading (Fe/Al $\leq$0.1) Al pairs are preferably balanced by bare Fe(II) cations, whereas at increasing Fe-loading the formation of iron oxo-dimers/polymers and, finally, of iron oxides is observed [10–17]. Although bare iron cations exhibit similar coordination and access similar rings both in MOR and FER topology, there are differences in their arrangement and surroundings which may cause a different exposition to the cavity and possible cooperation effects [18]. In the case of Fe-FER, both the high concentration of Al pairs and the local arrangement of the zeolite lattice are reflected in the high catalytic activity for the N_2O decomposition, if compared with Fe-ZSM-5, Fe-beta and Fe-MOR [12,19,20].

* Corresponding authors.
E-mail addresses: mariacristina.campa@cnr.it (M.C. Campa), edyta.tabor@jh-inst.cas.cz (E. Tabor).

https://doi.org/10.1016/j.apcatb.2023.123360
Received 29 June 2023; Received in revised form 25 September 2023; Accepted 3 October 2023
Available online 5 October 2023

Table 1
Iron-zeolites: starting material and analytical iron content.

Catalysts	Starting materials	wt.% Fe	$3Fe^{3+}/Al$
Fe-MOR-23	NH_4-MOR (Si/Al=9.2)	0.60	0.23
Fe-MOR-95	" "	2.47	0.95
Fe-FER-32	NH_4-FER (Si/Al=8.6)	0.79	0.32
Fe-FER-70	" "	1.70	0.70

DFT calculations evidenced in Fe-FER a specific arrangement of a couple of bare Fe(II) ions, called *distant binuclear cationic sites*, which are located in 6-membered rings (β cationic positions) and are axially oriented across the FER channels at a distance of 7.5 Å [18,21,22]. Thanks to the cooperation of the two Fe(II) sites in this peculiar arrangement, N_2O is easily split yielding reactive Fe(III)-O* (also referred to as $[Fe(IV)=O]^{2+}$) [10,12,18,19,21]. This is the well-known first step of the N_2O decomposition redox mechanism [23–26]. In the MOR framework, the possible occurrence of similar couples of bare Fe(II) ions at about 7.5 Å was also investigated by DFT calculations [18] but, due to their non-axial arrangement, they cannot successfully split N_2O. Since several spectroscopic studies on Fe-ZSM-5 [27,28], beta, and chabazite zeolites [29] showed the occurrence of Fe(II) dimeric species formed by Fe(II) ions at a closer distance of about 3 Å [27], in a previous investigation we suggested the presence of such dimeric $[Fe^{2+}$-□-$Fe^{2+}]$ species also in MOR, and we ascribed their poor reactivity towards N_2O decomposition to the formation of a stable Fe^{3+}-$O^{(1+\delta)-}$-$Fe^{(2+\delta)+}$ species, with a peculiar quasi-oxidic character [30]. Fe-MOR catalysts, although scarcely active for N_2O decomposition, are highly active for the selective catalytic reduction of N_2O with CH_4 [5,23] and Fe(II) dimers have been proposed as possible active sites [30]. It was also shown that in Fe-ZSM-5 and Fe-BEA the fraction of Fe(III) species inert in N_2O decomposition is easily reduced by the hydrocarbon present in the reaction mixture [31,32]. On Fe-MOR [5,23], Fe-ZSM-5 [33–36] and Fe-*BEA [32] the activity for N_2O reduction with hydrocarbon was widely investigated, whereas no significant data are reported for Fe-FER. Moreover, for MOR and FER, the location and nuclearity of the Fe-sites active for the N_2O abatement are still under debate and the influence of the topology and Al distribution on the iron speciation was not reported up to now.

With the aim of elucidating these aspects, in the present paper Fe-MOR and Fe-FER are investigated as catalysts for N_2O reduction with CH_4, focusing on the different iron speciation due to the MOR and FER topology. Specifically, Fe-MOR and Fe-FER samples with low (ca. 1 wt%) and high (ca. 2 wt%) Fe-loading were prepared to address the effect of iron-loading on the Fe speciation and on the catalytic performance. The same preparation method (*via* acetylacetone) was adopted for all samples, in order to avoid the influence of different protocols on the iron speciation. All catalysts were characterized by means of *in situ* UV–vis DRS and FTIR spectroscopies, investigating the reactivity of the Fe-sites with probe molecules (CO, NO, N_2O, CH_4). The activity for N_2O reduction with CH_4 (CR_{N2O}) was compared with that for decomposition (Dec_{N2O}), because these reactions, besides their practical interest, can be used as a probe to get information about the redox properties of iron species in zeolites. Since in real conditions O_2 and water vapour are always present, the catalysts have been investigated for N_2O reduction with CH_4 in the presence of excess of O_2 (SCR_{N2O}) and in hydrothermal conditions (water vapour addition to the reactant mixture). In this field, it is known that O_2 in the reaction mixture might compete with N_2O, while H_2O deactivated Fe-ZSM-5 and Fe-beta due to steam-dealumination followed by iron clustering [37]. Therefore, from the point of view of the potential application of this type of catalysts to N_2O abatement at the industrial level, the influence of the presence of O_2 and H_2O in the reaction mixture on both the nature of the iron species and the reaction mechanism has to be considered. In order to identify the surface species formed under reaction conditions, both in the absence and in the presence of water vapour, on all catalysts, *operando* FTIR experiments were carried out (steady-state or transient conditions) during CR_{N2O} and SCR_{N2O} reactions. The results of catalytic activity experiments and those of *operando* FTIR and *in-situ* UV–vis and FTIR studies were combined to get an insight into the nature of iron active sites, intermediates, and reaction pathways of the N_2O abatement.

2. Experimental methods

2.1. Catalysts preparation

Commercially available (Tosoh Corporation, Japan) mordenite (MOR) and ferrierite (FER) zeolites with Si/Al 9.2 and 8.6, respectively, were used as parent materials. The distribution of Al atoms in studied FER was determined previously [10,21]. In order to analyze the mordenite sample in terms of Al distribution, commercial MOR was first exchanged at room temperature (RT) with 1 M $NaNO_3$ to obtain Na-MOR. The Na-sample was repeatedly exchanged with 0.05 M $Co(NO_3)_2$ (three times for 24 h by 100 mL of a $Co(NO_3)_2$ solution *per* gram of zeolite at RT) to obtain maximally exchanged Co_{max}-MOR samples. The strictly followed conditions guaranteed the maximum exchange level of $[Co(II)(H_2O)_6]^{2+}$ ions (Co_{max}) without the occurrence of any hydrolytic Co complex [38–40].

For the preparation of Fe-FER and Fe-MOR samples, a previously described method was adopted [19,21]. MOR and FER zeolites were three times exchanged with NH_4NO_3 1 M (3 ×24 h at RT, 100 mL of a solution *per* 1 g of zeolite) to obtain ammonium form zeolites. Granulated NH^{4+}-MOR and NH^{4+}-FER were impregnated with $FeCl_3$ dissolved in acetylacetone and kept overnight. Then, the samples were evacuated and gradually heated up to 100 °C and 350 °C for 3 h. After cooling down, the samples were washed with distilled water and calcined at 450 °C overnight (*as prepared* samples). A series of two samples of iron mordenite and iron ferrierite with comparable low Fe-loading (below 1 wt%) and high Fe-loading (above 2 wt%) were prepared and denoted as Fe-MOR/FER-XX, where XX is the analytical Fe-exchange percentage, assuming that *one* Fe^{3+} corresponds to *three* Al atoms in the framework (Table 1).

2.2. Characterization techniques

Chemical analysis of Al and Co was performed using X-ray fluorescence spectroscopy (ARL 9400 XP, Thermo ARL, Switzerland), that of Fe by atomic absorption (Varian SpectrAA-220) after equilibrating sample at ca. 79% relative humidity over a saturated solution of NH_4Cl.

^{27}Al MAS NMR spectrum of hydrated Na-form of MOR was recorded at 11.7 T on a Bruker Avance III HD 500 WB/US spectrometer using 4 mm o.d. ZrO_2 rotors with a rotation speed of 7 kHz. The ^{27}Al isotropic chemical shifts were referenced to the aqueous solution of $Al(NO_3)_3$.

UV–vis diffuse reflectance spectra were recorded on *as prepared* Fe-MOR and Fe-FER samples in air in the wavenumber range of 4000–50000 cm^{-1} with a Varian Cary 5E spectrophotometer equipped with the integrating sphere for diffuse-reflectance measurements using HALON® as reference.

In situ UV–vis diffuse reflectance measurements were performed using a Perkin-Elmer Lambda 950 UV–Vis–NIR spectrometer equipped with the integrating sphere for diffuse-reflectance measurements covered by Spectralon®. Spectralon® also served as the reference. The absorptions were referred to the Schuster-Kubelka-Munk function $F(R\infty)=(1-R\infty)^2/2R\infty$, where $R\infty$ is the diffuse reflectance from a semi-infinite layer and $F(R\infty)$ is proportional to the absorption coefficient [17]. For determination of Al atoms distribution in MOR, UV–Vis spectra of maximum loaded Co-MOR were recorded after dehydration at 500 °C for 3 h. UV–vis spectra of Fe-FER and Fe-MOR samples were recorded after the following treatments: i) 3 h evacuation under dynamic vacuum at 500 °C, measurement of sample under vacuum at RT, ii) 10 min interaction with N_2O at 250 °C, measurement at RT in N_2O atmosphere, iii) N_2O desorption at RT for 2 min, measurement at RT under vacuum, iv) 10 min interaction with CH_4 at 250 °C, measurement at RT in CH_4

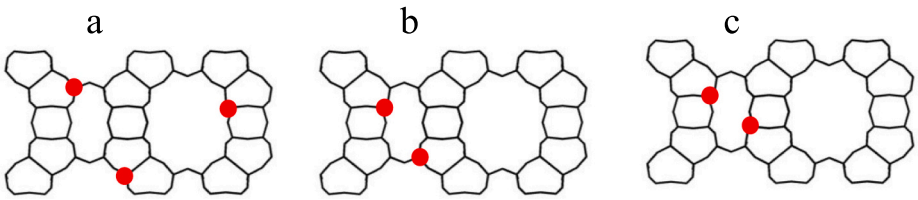

Fig. 1. Schematic representation of organization of Al atoms in MOR as single Al atoms (Al_{1Al}) (a) and as Al pairs (Al_{2Al}) (b) and (c).

atmosphere, v) CH_4 desorption at RT for 2 min, measurement under vacuum at RT.

FTIR spectra were recorded by a spectrometer Perkin Elmer Frontier, equipped with a MCT detector, operating at a resolution of 4 cm^{-1}. The powdered samples were pressed (pressure, 2 $\times 10^4$ Kg cm^{-2}) to obtain self-supporting wafers of about 20 mg (10 mg cm^{-2}). For *in situ* FTIR measurements with probe molecules, sample wafers were put in a quartz cell, provided with KBr windows, which allowed thermal treatments in a vacuum or in a controlled atmosphere. Before adsorption of NO (AIR LIQUIDE/SIO, 99.0%) or CO (SOL, 99.9%) at RT samples were activated by evacuating up to 200 °C, heating in O_2 (SOL, 99.9%) up to 500 °C for 1 h and evacuating at the same temperature for 1 h. For the *operando* FTIR experiments, sample wafers were put in a stainless-steel reactor, equipped with CaF_2 windows, that allowed to record spectra up to 500 °C, under gas stream. The IR reactor was connected to the flow apparatus we used for catalytic measurements, and reactants and products were analyzed by the online gas-chromatograph. Samples were activated under O_2/He flow (2.5% v/v), cooled to the desired temperature under He flow, and exposed to the feeding mixtures, having the same composition and total flow rate as that we used for catalytic experiments. Spectra were recorded at various temperatures (steady-state experiments) or as a function of time on stream at a constant temperature (transient experiments). Spectra recorded after heating samples in the He stream at a given temperature (blank experiments at 25–500 °C) were subtracted from those obtained after heating in the reactant mixture stream at the same temperature.

2.3. Catalytic tests

The catalytic activity was measured in a flow apparatus at atmospheric pressure in steady-state conditions using a quartz reactor. The apparatus included a feeding section where four gas streams (He, 3% N_2O in He, 1.5% CH_4 in He, 10% O_2 in He) were regulated by independent mass flow controller-meters (MKS) and mixed in a glass ampoule before entering the reactor. Gas mixtures were purchased from RIVOIRA and used without further purification. Reactants and products were analyzed by a gas-chromatograph (Agilent 7890 A GC system) equipped with three columns (Molsieve 5 A, for detecting O_2, N_2 and CO, Porapack Q for detecting CO_2 and N_2O, and Na_2SO_4 doped alumina for detecting CH_4) and two detectors (TCD and FID). Experiments yielded satisfactory nitrogen and carbon balances (within the experimental error). A portion of sample (0.100 g) was activated by feeding 2.5% O_2/He mixture (100 cm^3 min^{-1}) from RT to 500 °C and then maintaining isothermally at 500 °C for 90 min. After this treatment, the reactor was bypassed and the temperature adjusted to the desired value. In a typical catalytic run the reaction temperature was changed at random without intermediate activation treatment. Catalysis was run by contacting the catalyst with feeds of various composition (v/v, He as balance): N_2O, N_2O+H_2O, N_2O+CH_4 (CR_{N2O}), N_2O+CH_4+O_2 (SCR_{N2O}), N_2O+CH_4+O_2+H_2O, and CH_4+O_2. The concentration was 4000 ppm for N_2O and CH_4 and 20,000 ppm for O_2 and H_2O. The total flow rate was maintained at 50 cm^3 STP/min, and gas hourly space velocity (GHSV) was 15,000 h^{-1}, based on the apparent sample density of 0.5 g cm^{-3}. For all the reactions, the catalyst was stable as a function of the time on stream, throughout experiments lasting up to about 8 h. Conversions obtained at various (sample weight)/(flow rate) ratios (W/F) indicated that, in our conditions, reaction is under kinetic control without diffusion effect.

Percent conversion of N_2O or CH_4 was calculated as 100•(molecules consumed)/(molecules injected). Percent selectivity of CO_2 was calculated as 100•(CO_2 molecules formed)/(CO_2+CO molecules formed). The N_2O/CH_4 ratio was calculated as (N_2O molecules consumed)/(CH_4 molecules consumed) and the O_2/CH_4 ratio as (O_2 molecules consumed)/(CH_4 molecules consumed). The reaction rate of N_2O consumption (r_{N2O} / molecules s^{-1} g^{-1}) and apparent activation energy values (E_a / kJ mol^{-1}) were calculated from experiments in which conversion values did not exceed 30% (log r_{N2O} vs. 1/T).

3. Results and discussion

3.1. Al atoms organization in parent MOR zeolite

Single pulse ^{27}Al MAS NMR spectrum of hydrated Na-MOR exhibited the intense maximum with the observed shift of 55 ppm reflecting the locations of the Al atoms in various framework tetrahedral T (Si, Al) sites, while ^{27}Al chemical shifts of Oh-coordinated Al atoms (^{27}Al observed shift around 0 ppm) and perturbed Td-coordinated Al (^{27}Al observed shift from 30 to 40 ppm) were not observed (Supplementary Materials, Fig. S1). This confirmed that Al atoms are exclusively located in the framework positions of MOR sample [10,21], within the detection limits of this technique (1–5%). For FER matrix, ^{27}Al MAS NMR studies previously evidenced the exclusive presence of Td coordinated Al atoms in the framework and the absence of extra-framework Al atoms [10,21,39].

In high-silica zeolites, framework Al are organized as single Al atoms (Al_{1Al}, Fig. 1a), i.e. one Al atom in the ring, or as a pair of Al atoms corresponding to two Al atoms in one ring (Al_{2Al}) separated by two or three silicon atoms (Figs. 1b, 1c) [18]. In the case of FER and MOR, only the rings with two Al atoms are able to host both Co(II) hexa-aquacomplex in the hydrated form of zeolite and bare divalent cations in the dehydrated zeolite [8,9]. Close Al atoms (two Al atoms in two close rings) are only able to balance Co(II) hexa-aquacomplex but not bare divalent cations, and up to now are reported only for beta and SSZ-13 zeolites [9,41]. Therefore, the total content of aluminum atoms (Al_{total}, from atomic absorption spectroscopy), can be expressed by eq. Eq. 1:

$$Al_{total} = Al_{2Al} + Al_{1Al} \quad (1)$$

Due to the fact that in FER and MOR topology several rings contains Al pairs capable to accommodate bare divalent cations, three cationic sites of divalent species were suggested for these matrices: (i) β cationic site (A position in Mortier notation), corresponding to the 6MR of the FER side channel and twisted 8MR forming bottom of the MOR pocket, (ii) α-site, related to the 6MR in the main channel of FER (B position in Mortier notation) and MOR structure (E position in Mortier notation), and (iii) less populated γ-site (C position in Mortier notation), corresponding to Al_{2Al} pairs in so-called boat-shaped ring inside the FER side channel and MOR pocket [42–47].

The determination of the Al atoms distribution in MOR zeolite investigated in this study was based on the application of Co(II) ions as probes monitored by UV-vis spectroscopy supported by quantitative

Table 2
Chemical composition, maximum ion-exchange capacity of Co(II) (Co_{max}), concentrations of Al in Al_{2Al} and Al_{1Al} in parent MOR and FER zeolites.

Sample	Si/Al	Al_{total} [a]	Co_{max} [a]	Co_{max}/Al_{total}	Al_{2Al}		Al_{1Al}	
	molar ratio	mmol g^{-1} [a]	mmol g^{-1} [a]	molar ratio	mmol g^{-1} [a]	%	mmol g^{-1} [a]	%
MOR	9.2	1.67	0.60	0.36	1.20	72	0.47	28
FER[10]	8.6	1.65	0.55	0.33	1.09	66	0.56	34

[a] Data obtained from chemical analysis.

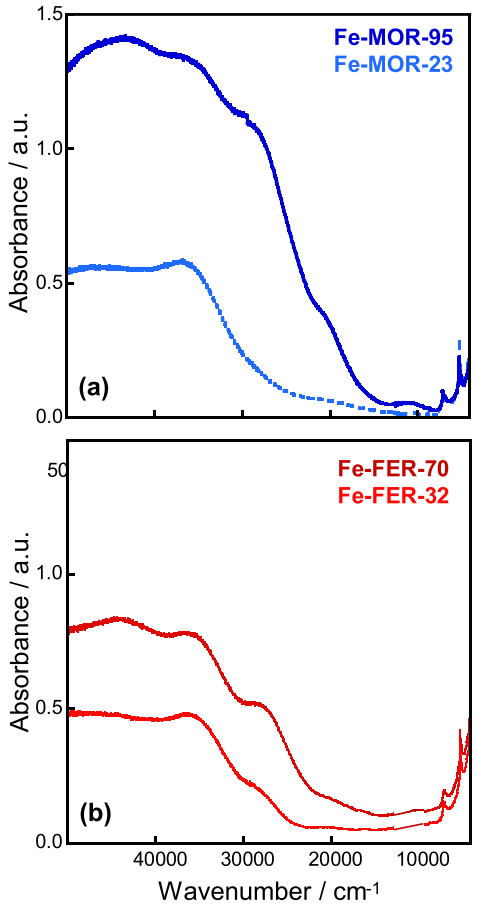

Fig. 2. UV–vis spectra of as prepared Fe-MOR (Section a) and Fe-FER catalysts (Section b).

data from chemical analysis. The Co(II) can be exchanged in the Na-zeolite as Co(II) hexa-aquocomplex by using controlled conditions of the ion-exchange procedure which do not involve hydrolysis reactions and lead to the stabilization of one bare Co(II) by Al_{2Al} pair in the dehydrated sample [8,9,48,49]. For Co-MOR samples obtained following this standardized procedure, the UV–vis spectrum (Supplementary Materials, Fig. S2) exhibited the typical d-d transitions ranging from 14000 to 25000 cm^{-1} representing bare Co(II) ions located in cationic sites (α, β, and γ) coordinated only to framework oxygen atoms in zeolite rings with Al_{2Al} pairs [50], and bands above 40000 cm^{-1} reflecting Co(II)-O charge transfer of bare Co(II) ions and Al-O and Si-O. CT bands below 40000 cm^{-1} attributable to the Co-oxo species were not observed. Therefore, the concentration of Al atoms as Al_{2Al} pairs in 6MRs of zeolite is twice the concentration of Co_{max} (one Co(II) is stabilized by two Al atoms in one ring) [8], according to Eq. 2:

$$[Al_{2Al}] = 2\ Co_{max} \quad (2)$$

The value of Co_{max}, based on the results from chemical analysis, revealed that MOR matrix contained majority (72%) of Al atoms forming Al pairs. This type of Al distribution is crucial for stabilization of divalent cations, which are suggested as catalytically active centers in redox reactions. The rest (28%) of Al atoms in MOR matrix was present as single atoms (Al_{1Al}). The comparison of these results with those previously obtained on FER (Table 2) indicated that our MOR and FER matrices exhibited a similar concentration and distribution of Al atoms, which were mainly organized as pairs in both zeolite structures. This type of Al distribution is crucial for the stabilization of divalent cations. In our study, since the number of divalent cations that can be stabilized by the two MOR and FER structures is similar, the formation of active centers, their nature, and reactivity as a function of iron loading could be related to the zeolite topology in combination with the position of Al pairs in the framework.

3.2. Iron speciation

The co-existence of Fe(III) and Fe(II) in thermally activated Fe-zeolites prepared by using Fe(III) salts is by consensus reported in the literature [10,17,19,31,51]. It was also shown that the method of iron introduction with the use of acetylacetone as the solvent is very efficient in providing the occupation of the cationic positions of iron in zeolites (FER, *BEA, and MFI)[10,19,21] and for this reason the same method was also extended to Fe-MOR in the present work. Mössbauer studies confirmed that iron zeolites prepared by using this method with Fe/Al < 0.1 contained predominantly ($> 70\%$) Fe(II) species [18,19,22,52].

In order to determine the influence of the iron content on the formation of particular iron species, Fe-FER and Fe-MOR samples with similar low iron loading (Fe/Al ≤ 0.1) and high iron loading (Fe/Al ≥ 0.2) were studied. Samples with low iron loading in which iron is mainly observed as bare cation [10–16] are suitable for spectroscopic studies to get an insight into the role of Al atoms for the stabilization of these bare species, while samples with a higher amount of iron allow to observe the formation of additional iron sites.

3.2.1. Fe(III) speciation by UV–vis spectroscopy in as prepared samples

The UV–vis spectra of *as prepared* low- and high-loaded Fe-MOR and Fe-FER revealed the nature of Fe(III) species formed in the Fe zeolites of different topology (Fig. 2). The complex intense bands in the region 18000–50000 cm^{-1} (charge-transfer transitions, CT, O→Fe(III)) observed in the spectra of all samples indicated the heterogeneity of Fe (III) species, which were present as isolated Fe(III) in tetrahedral (Td) or octahedral (Oh) coordination, and as dinuclear and polynuclear Fe(III) species [17,23,51,53]. Since the nuclearity of polynuclear Fe(III) species is correlated with the number of Fe-O bonds, the higher number of Fe-O bonds in the oligomeric structure the lower value of charge transfer energy [51].

The UV–vis spectrum of low-loaded Fe-MOR-23 (Fig. 2a) and Fe-FER-32 (Fig. 2b) both exhibited a poorly resolved absorption at around 47,000 cm^{-1} and a well-developed band at 37,000 cm^{-1}, typical of ligand-to-metal CT of isolated Oh and Td Fe(III) species [51,53], and a shoulder at 28,000 cm^{-1}, more defined in Fe-FER-32, due to di-nuclear or poly-nuclear Fe(III)-oxo complexes [17,54,55]. The UV–vis spectrum of both high-loaded Fe-MOR-95 and Fe-FER-70 showed that the introduction of a higher amount of iron into the zeolites led to the increase of all absorptions from Fe(III) species from isolated and di/poly-nuclear Fe-species, more defined in Fe-FER-70 and more intense in Fe-MOR-95. This implies that despite the similar concentration of Al pairs in the MOR and FER matrix, the MOR matrix stabilized a higher

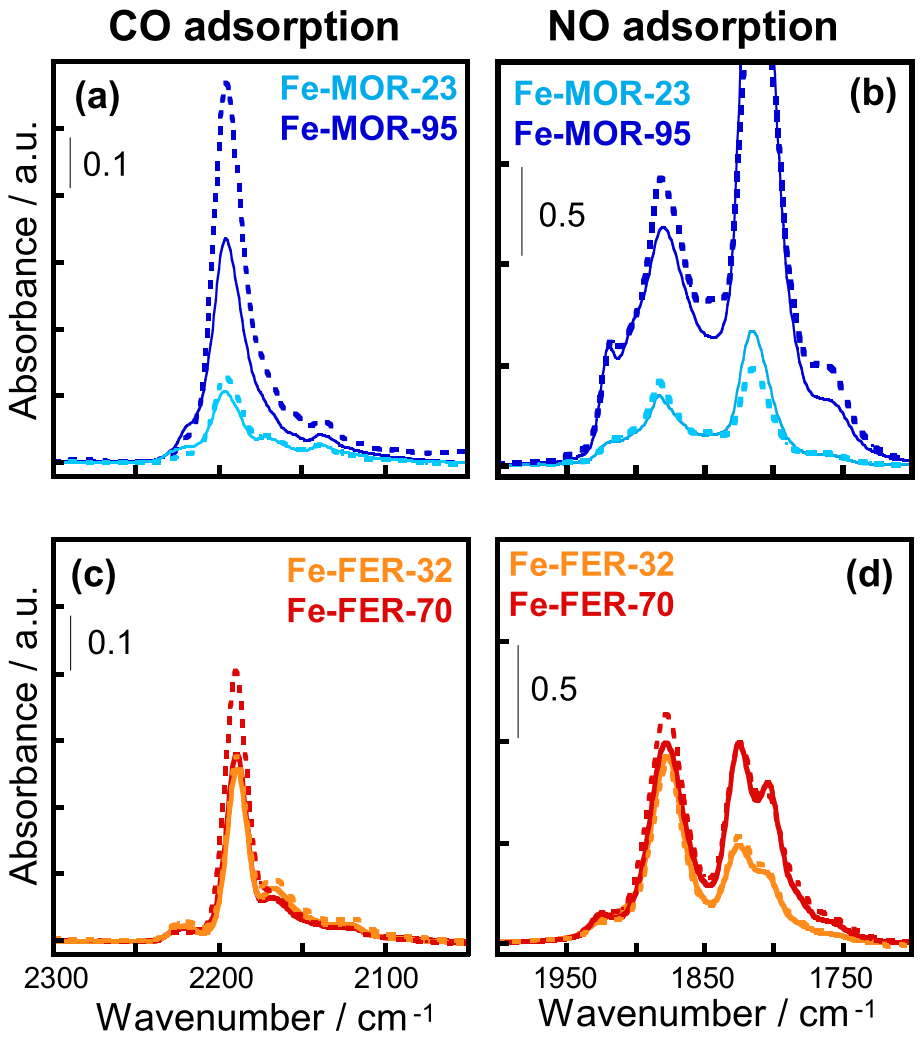

Fig. 3. *In situ* FTIR spectra of CO (Sections a and c) or NO (Sections b and d) adsorbed at RT (equilibrium $P_{CO} \cong P_{NO} \cong 100$ Torr) on activated Fe-MOR (Sections a and b) and Fe-FER catalysts (Sections c and d) at different Fe-loading. Experiments on samples pre-reduced by CO at 320 °C were also reported (dotted-line spectra). Samples were heated in CO from RT up to 320 °C, kept for 5 min at 320 °C, and cooled to RT, before recording spectra in the presence of CO or NO. In Section b, the band at about 1800 cm^{-1} is out of scale.

population of Fe(III) species more heterogeneous in comparison to FER.

All Fe-MOR and Fe-FER samples were free from iron oxide clusters, due to the very small absorption below 20,000 cm^{-1}. It could be concluded that the employed method for the introduction of iron in MOR and FER samples (*via* acetylacetone) led to the formation of different families of well-dispersed isolated iron sites and Fe(III)-oxo species with low nuclearity.

The presence of Fe(II) is not expected in *as prepared* samples because, as explained in the forthcoming sections, this species is formed after the activation treatment. Moreover, Fe(II), if present, would be scarcely detectable by UV–vis spectroscopy because its *d-d* transitions in this kind of samples turn out to be very weak and its CT transitions are generally covered by those of Fe(III) [27].

3.2.2. *Fe(II) speciation by in situ FTIR spectroscopy*

3.2.2.1. CO and NO adsorption on activated samples. In both activated Fe-MOR and Fe-FER samples the adsorption at RT of CO and NO as probe molecules revealed the formation of Fe(II) species. As already established in previous studies [10,17,19,28,31,51], these species probably originated from the most reducible Fe(III)-oxo species that underwent reduction during thermal treatments in the preparation and activation procedures and are hereafter indicated as $Fe(II)_{ACT}$. The peculiarity of $Fe(II)_{ACT}$ species is that they are obtained by thermal treatment under vacuum or even in a mild oxidizing environment (O_2/He flow, 2.5 %) [23,28].

Adsorption of CO on activated Fe-MOR-23 and Fe-MOR-95 (Fig. 3a) led to the formation of carbonyl bands at 2225, 2200, 2175, and 2130 cm^{-1}. The most intense band centered at 2200 cm^{-1} represents stable Fe(II)-CO complexes on sites with electrophilic character. The weak band at 2225 cm^{-1} arose from a small contribution of Al(III)-CO species. The band at 2175 cm^{-1}, which only appeared as a shoulder in Fe-MOR-95, was due to CO polarized by the residual acidic hydroxyls, and the low-intensity band at 2130 cm^{-1} was typical of physisorbed CO [56,57]. The intensity of the Fe(II)-CO bands in Fe-MOR significantly increased with increasing Fe-loading, indicating that in the MOR matrix the specific cationic positions accessible to Fe(II) were gradually populated at increasing iron concentration.

In activated Fe-FER-32 and Fe-FER-70 CO adsorption (Fig. 3c) revealed bands similar to those in Fe-MOR and corresponding to Fe(II)-CO species (2196 cm^{-1}), Al(III)-CO (2225 cm^{-1}), CO polarized by the acidic hydroxyls (2170 cm^{-1}), physisorbed CO (2120 cm^{-1}). By comparing Fe-FER-32 and Fe-FER-70 spectra, the intensity of the Fe(II)-CO band (2196 cm^{-1}) did not increase with Fe-loading, suggesting that,

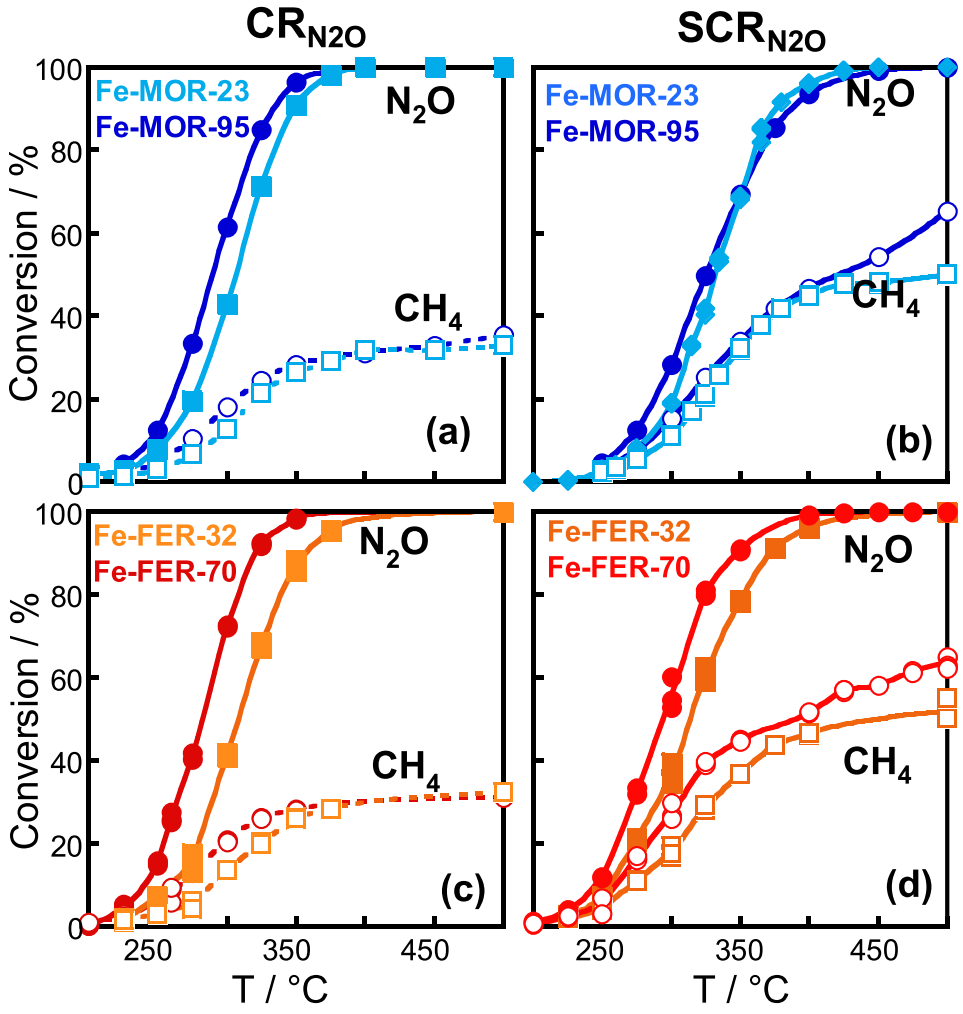

Fig. 4. CR_{N2O} (Sections a and c) and SCR_{N2O} reactions (Sections b and d) on Fe-MOR (Sections a and b) and Fe-FER catalysts (Sections c and d) at different Fe-loading. Percent N_2O and CH_4 conversion as a function of temperature. Reactant concentration: $[N_2O]= [CH_4]= 0.4\%$, $[O_2]= 0$ or 2% (total flow rate=50 cm^3 STP/min, He as balance).

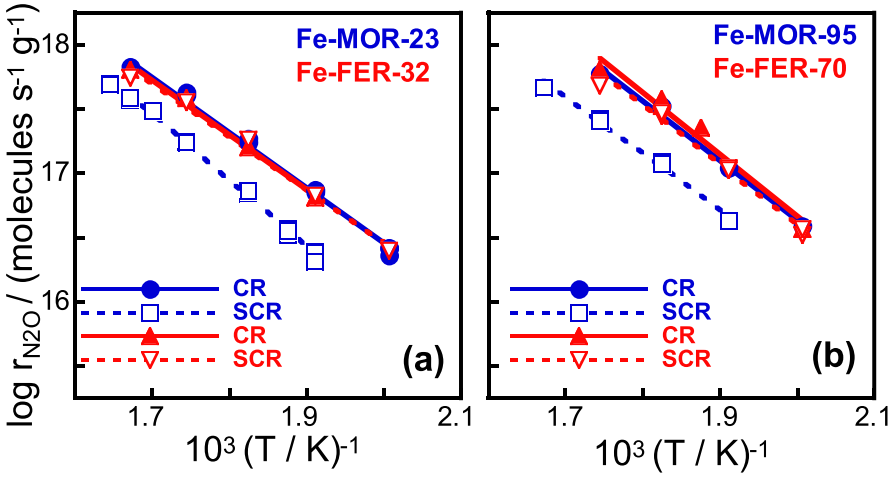

Fig. 5. The comparison between CR_{N2O} and SCR_{N2O} on low-loaded (Section a) and high-loaded (Section b) Fe-MOR and Fe-FER catalysts. Arrhenius plot, log r_{N2O} vs. 1/T (r_{N2O} / molecules s^{-1} g^{-1}). Catalysts and reactions as indicated.

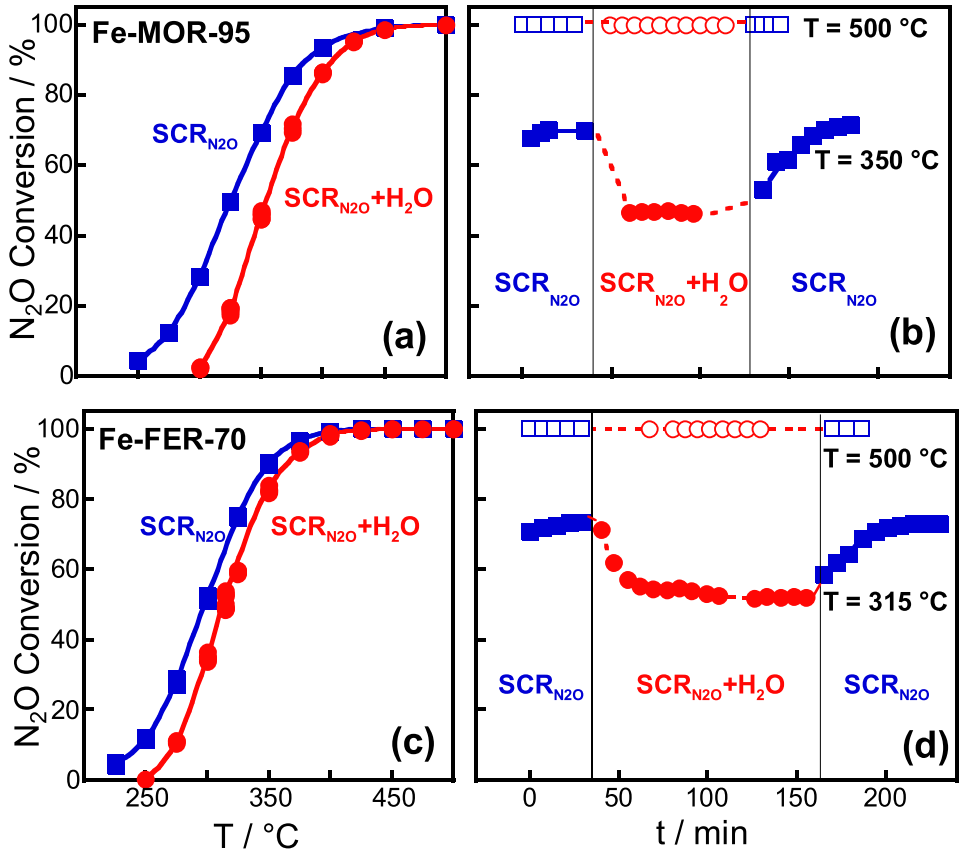

Fig. 6. SCR_{N2O} reaction on Fe-MOR-95 (Sections a and b) and Fe-FER-70 (Sections c and d), in the presence or in the absence of H_2O vapor in the reactant mixture. Percent of N_2O conversion as a function of temperature (Sections a and c) and of time on stream at set temperatures as indicated (Sections b and d). Reactant concentration: $[N_2O]= [CH_4]= 0.4\%$, $[O_2]= 2\%$ and $[H_2O]= 0$ or 2%; (total flow rate=50 cm^3 STP/min, He as balance).

differently from the MOR matrix, in the FER matrix the saturation of specific cationic positions by Fe(II) is reached already at low iron-loading. While the carbonyl band was much more intense in Fe-FER-32 than in Fe-MOR-23, the same band was somewhat more intense and broader in Fe-MOR-95 than in Fe-FER-70 (Supplementary Materials, Fig. S3). These results indicated the influence of the matrix topology on the ability to stabilize different types of $Fe(II)_{ACT}$ sites, despite the similar concentration of Al pairs in FER and MOR matrices, the FER matrix strongly stabilized more homogeneous $Fe(II)_{ACT}$, already at low iron-loading. Moreover, the position of Fe(II)-CO band was at slightly lower wavenumbers in FER than in MOR (Fig. S3), suggesting a slightly lower Lewis acidity of $Fe(II)_{ACT}$ sites in FER than in MOR.

The NO adsorption was used to better evaluate the speciation of Fe (II), due to the NO strong affinity toward Fe(II) that results in the formation of stable nitrosyl species [58].

Regardless of the type of zeolite matrix, on the activated Fe-MOR and Fe-FER samples NO adsorption yielded several nitrosyl bands (intense bands of ν_{NO} in the 1950–1700 cm^{-1} region, Fig. 3b and d) that evidenced different types of $Fe(II)_{ACT}$ sites. Additionally (Supplementary Materials, Fig. S4), on all samples NO disproportionation involving surface OH occurred as a side process, as suggested by a coupled negative and positive absorptions in the OH stretching region (3800–3000 cm^{-1}) and by the bands from adsorbed N_2O (peak of $\nu_{N\equiv N}$ at 2250 cm^{-1}), NO^+ (band at 2170 cm^{-1}), and nitrates (1650–1550 cm^{-1}) [59–61].

For Fe-MOR samples, the analysis of the nitrosyl bands region (Fig. 3b) showed (i) an intense band at 1880 cm^{-1} with a shoulder at about 1910 cm^{-1}, both reaching a plateau at increasing NO pressure, the latter at low coverage (Supplementary Materials, Fig. S5), indicating two types of Fe(II)-NO mononitrosyl species, (ii) a weak component at 1760 cm^{-1}, ascribed to Fe-$(NO)_2$ dinitrosyls , and (iii) bands at 1820 and 1925 cm^{-1}, typical of Fe-$(NO)_3$ trinitrosyl species with symmetry lower than C_{3v} [5,62]. On this basis, at least three types of $Fe(II)_{ACT}$ species in different positions of MOR cavities can be inferred, two species enable to adsorb at maximum one molecule of NO, and a third species filling its coordination sphere with two or three NO molecules, depending on the pressure of NO. At increasing Fe-loading in MOR matrix, the intensity of all nitrosyl bands increased, indicating that the amount of $Fe(II)_{ACT}$ species increased (Fig. 3b), in agreement with the CO adsorption result.

Also in Fe-FER samples (Fig. 3c), as in Fe-MOR, several types of Fe $(II)_{ACT}$ species can be identified: the intense band at 1877 cm^{-1} was assigned to a Fe(II)-NO species; the band at 1760 cm^{-1} corresponds to the low-frequency mode of the Fe(II)-$(NO)_2$ species (being the high-frequency one at about 1840 cm^{-1} not resolved in the spectrum); the bands at 1825 and 1805 cm^{-1} coupled with the shoulder at 1920 cm^{-1} to a Fe(II)-$(NO)_3$ species (these latter bands increased in parallel with NO pressure, see Supplementary Materials, Fig. S5) [60,63–66]. Unlike in Fe-MOR, where two types of Fe(II)-NO species have been deduced, in Fe-FER only one type of Fe(II)-NO species was revealed as indicated by the symmetrical shape of the corresponding band. Moreover, in Fe-FER the Fe(II)-$(NO)_3$ species displays more distorted C_{3v} symmetry than in MOR, as two components at 1825 and 1805 cm^{-1} are detectable in Fe-FER whereas only one component at around 1820 cm^{-1} is present in Fe-MOR.

Therefore, the comparison of NO adsorption results obtained on Fe-FER and Fe-MOR samples with similar iron loading (Supplementary Materials, Fig. S6) evidenced that the matrix topology controlled the Fe $(II)_{ACT}$ speciation with respect to the coordinative unsaturation and to the symmetry of the stabilized Fe(II) sites. In particular, in Fe-FER (i) Fe (II)-mononitrosyl species are less heterogeneous than in Fe-MOR and the

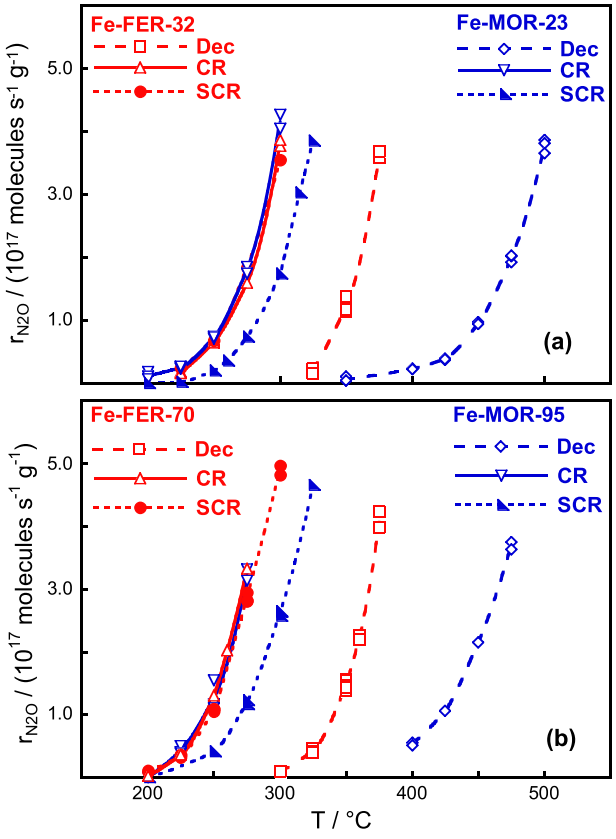

Fig. 7. The comparison between the N_2O abatement rate (r_{N2O} / molecules s^{-1} g^{-1}) in N_2O decomposition, CR_{N2O} and SCR_{N2O} as a function of temperature. Low-loaded (Section a) and high-loaded (Section b) Fe-MOR and Fe-FER catalysts, as indicated. Reactant concentration: $[N_2O]$= $[CH_4]$= 0.4% and $[O_2]$= 2% (total flow rate=50 cm^3 STP/min, He as balance).

relative amount Fe(II)-mononitrosyl/Fe(II)-polynitrosyls is higher. Moreover, at increasing Fe-loading, while in Fe-MOR the amount of all nitrosyl species increased, in Fe-FER the amount of Fe(II)-NO did not. This finding indicates that the $Fe(II)_{ACT}$ species capable to adsorb only one NO molecule are introduced in FER matrix at low Fe-loading, while $Fe(II)_{ACT}$ species with more coordinative unsaturations capable to adsorb two or three NO molecules are introduced at higher loading. This evidence confirmed that the FER matrix strongly stabilized peculiar Fe (II) sites, those with low coordinative unsaturations (able to adsorb only one NO molecule), that are populated already at low Fe-loading.

3.2.2.2. NO and CO adsorption on samples reduced by heating in CO. On both Fe-MOR-95 and Fe-FER-70 high-loaded catalysts, besides $Fe(II)_{ACT}$ formed by thermal activation, additional Fe(II) species were formed by a thermal treatment with CO or CH_4 as reductants and are hereafter indicated as $Fe(II)_{RED}$. Those reduced after CO thermal treatment coordinate CO molecules and give rise to the spectra corresponding to the dotted lines in Figs. 3a and 3c.

Specifically, the adsorption of CO on samples heated in CO at 320 °C yielded a Fe(II)-CO band more intense than in activated samples and the appearance of linearly-adsorbed CO_2 band (ν_{OCO} at 2350 cm^{-1}). These evidences suggested that Fe(III)-oxo species containing a reactive extra-lattice O atom (as Fe(III)-O-Fe(III) dimers) underwent reduction by CO yielding CO_2 and $Fe(II)_{RED}$ species (Fe(II)-□-Fe(II), in the case of dimers) able to form new Fe(II)-CO carbonyls. The NO adsorption on both Fe-MOR-95 and Fe-FER-70 high-loaded catalysts reduced in CO at 320 °C, yielding Fe(II)-nitrosyl bands more intense than those observed in activated samples (dotted spectra in Fig. 3b and d), confirmed the previous suggestion that an additional fraction of Fe(II) species, $Fe(II)_{RED}$, formed from Fe(III)-oxo species by a reductant treatment.

On low-loaded samples, the reductant treatment caused a small (Fe-MOR-23) or negligible (Fe-FER-32) increase of carbonyl and nitrosyl bands (Fig. 3), indicating that a small amount of $Fe(II)_{RED}$ was formed by reduction on Fe-MOR and none on Fe-FER, suggesting that on Fe-FER-32 probably all Fe(II) species were stabilized already by activation, $Fe(II)_{ACT}$.

3.3. Catalytic activity

3.3.1. Catalytic activity for N_2O reduction with CH_4 in the absence and in the presence of O_2

For N_2O reduction with CH_4 in the absence of O_2 (CR_{N2O}) all catalysts were highly active, with a light-off temperature of about 200 °C. N_2O conversion reached 100% in the range 350–400 °C, at which CH_4 conversion reached its maximum value (about 30%), remaining constant at higher temperature (Fig. 4a and c). At increasing Fe-content, the activity increased nearly proportionally on Fe-FER, and less on Fe-MOR catalysts.

To clarify the reactions occurring in the CR_{N2O} process, we combined the N_2O/CH_4 ratio values with the selectivity to CO_2 (S_{CO2}). On all catalysts the N_2O/CH_4 ratio as a function of temperature was in the range 2.4–3.9 and the selectivity S_{CO2} was in the range 27–60% (Supplementary Materials, Fig. S7a and c), indicating that, in addition to the expected reactions $CH_4 + 4\ N_2O \rightarrow 4N_2 + CO_2 + 2\ H_2O$ and $CH_4 + 3N_2O \rightarrow 3\ N_2 + CO + 2\ H_2O$, side-reactions yielding H_2 had to be considered to justify the N_2O/CH_4 values lower than 3: $CH_4 + 2N_2O \rightarrow 2N_2 + CO_2 + 2H_2$ and $CH_4 + N_2O \rightarrow N_2 + CO + 2H_2$. However, the occurrence in a low extent of reactions yielding other C-byproducts could not be excluded, because on catalysts at low Fe-loading the C-balance lower than 100% (≥90%) indicated the formation of GC-undetectable species.

When excess O_2 was added to the N_2O+CH_4 mixture (SCR_{N2O}), both Fe-MOR and Fe-FER systems were still highly active for N_2O reduction with CH_4 (Fig. 4b and d). At increasing Fe-loading, the N_2O conversion increased on Fe-FER and little on Fe-MOR.

As on both series of Fe-FER and Fe-MOR catalysts in the temperature range 250–400 °C (i) the N_2O/CH_4 ratio was about 2 and O_2/CH_4 ratio about 1–0.75, (ii) the selectivity to CO_2 was in the range 20–80% (Supplementary Materials, Fig. S7b and d), and (iii) C- and N-balance were about 100%, these values indicated that SCR_{N2O} occurred with the following stoichiometries, $CH_4 + 2N_2O + O_2 \rightarrow 2N_2 + CO_2 + 2H_2O$ and $CH_4 + 2N_2O + 1/2O_2 \rightarrow 2\ N_2 + CO + 2H_2O$. At temperature higher than 400 °C, on the high-loaded Fe-FER-70 and Fe-MOR-95 the N_2O/CH_4 values decreased to 1.7 and 1.5 respectively, suggesting that while at low temperature O_2 participated to the N_2O reduction pathway, at higher temperature combustion as side-reaction also occurred to a small extent.

The comparison between the catalytic activity of Fe-MOR and Fe-FER catalysts showed that the N_2O abatement in CR_{N2O} negligibly depended on the matrix (Fig. 5a and b), suggesting similar amounts of Fe (II) working sites at similar Fe-loading. Differently, the N_2O abatement in SCR_{N2O} was higher on Fe-FER than on Fe-MOR catalysts (Fig. 5a and b).

The comparison between SCR_{N2O} and CR_{N2O} results, besides a detrimental effect of O_2 on the reductant efficiency (N_2O/CH_4 ratio markedly decreased passing from CR_{N2O} to SCR_{N2O}, see Supplementary Materials, Fig. S7), showed a different O_2 effect on the N_2O reduction rate in the two systems. Specifically, in both Fe-FER catalysts the reaction rate was not affected by the O_2 in the feed (similar values of log r_{N2O} *vs* 1/T for SCR_{N2O} and CR_{N2O}), whereas in both Fe-MOR catalysts a detrimental effect of O_2 on the activity was observed, as in fact the rates were lower in SCR_{N2O} than in CR_{N2O} (Fig. 5).

3.3.1.1. SCR_{N2O} in hydrothermal conditions. In order to verify if Fe-MOR

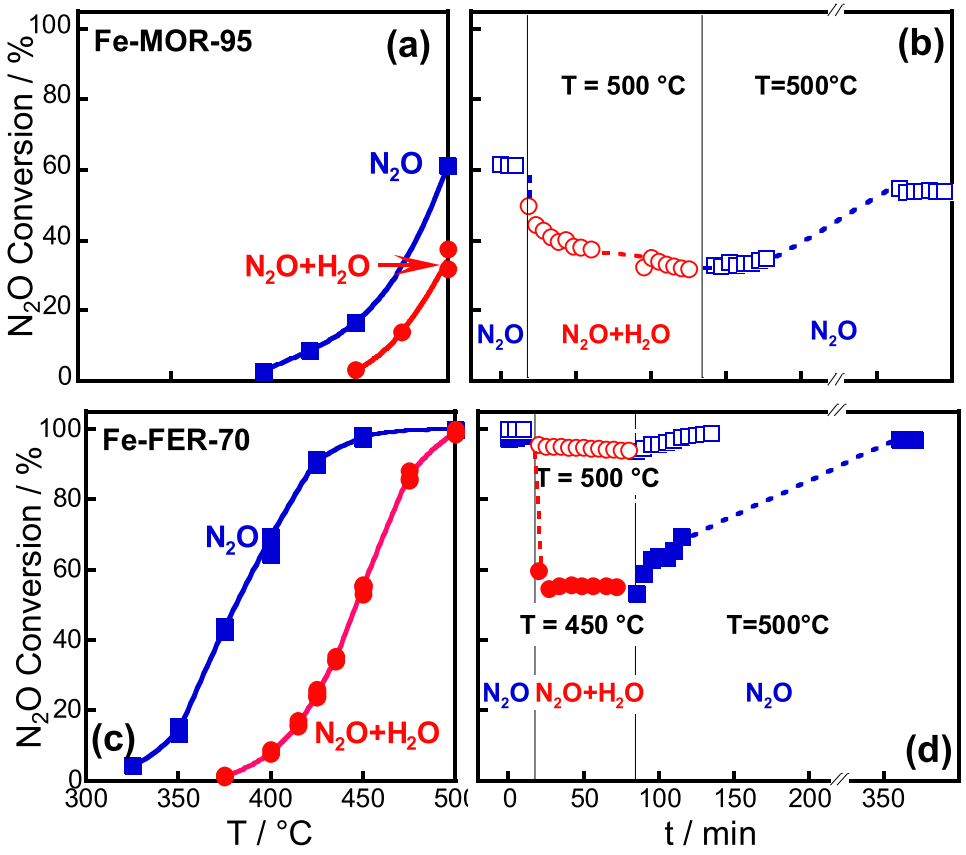

Fig. 8. N_2O decomposition on Fe-MOR-95 (Sections a and b) and Fe-FER-70 (Sections c and d), in the presence or in the absence of H_2O vapor in the reactant mixture. Percent of N_2O conversion as a function of temperature (Sections a and c) and of time on stream at set temperatures as indicated (Sections b and d). Reactant concentration: [N_2O]= 0.4% and [H_2O]= 0 or 2% (total flow rate=50 cm^3 STP/min, He as balance). In Sections b and d, the activation treatment consists in heating the samples at 500 °C for more than 3 h in flow mixture.

and Fe-FER systems were stable under real feeds, we investigated the activity, the stability and the reversibility of the catalytic activity for SCR_{N2O} after addition of water vapor (about 20000 ppm) to the feed. After the H_2O addition the activity slightly decreased on both Fe-MOR-95 and Fe-FER-70 catalysts in the whole temperature range (Fig. 6a and c). In particular, at the temperature at which the N_2O conversion in dry feed was about 70% (350 °C for Fe-MOR-95 and 315 °C for Fe-FER-70), the conversion decreased to about 50% after H_2O addition, but it remained stable as a function of time on stream (Fig. 6b and d). This result suggested that only a fraction of the active sites was poisoned. On both catalysts, the activity was reversibly restored in about 30 min when H_2O was eliminated from the feed, suggesting that deactivation by H_2O was due to a reversible poisoning (H_2O adsorption/desorption). In agreement, at higher temperature (500 °C), where the coverage by H_2O was probably negligible, the activity did not decrease and remained stable as a function of time on stream (Fig. 6b and d). These results excluded the occurrence of Fe-oxide segregation during SCR_{N2O} in the presence of H_2O.

3.3.2. *N_2O abatement related reactions: CH_4 combustion and N_2O decomposition*

In order to have a better insight into the different behaviour of the Fe-zeolites for CR_{N2O} and SCR_{N2O} we studied the CH_4 combustion and N_2O decomposition reactions that involved the activation of the reactants.

CH_4 combustion occurred only on high-loaded Fe-MOR-95 and Fe-FER-70 catalysts above 400 °C and to a similar extent (about 40% of CH_4 conversion at 500 °C, Supplementary Materials, Fig. S8a). Since CH_4 conversion in CR_{N2O} and SCR_{N2O} reactions started well below 400 °C (200–250 °C, see Fig. 4), CH_4 activation below 400 °C required N_2O.

For N_2O decomposition, Fe-FER catalysts were markedly more active than Fe-MOR catalysts (Fig. 7 and Supplementary Materials, Fig. S8b), being the former active above 300 °C and the latter above 375 °C. Since at increasing Fe-loading the activity increased in Fe-MOR whereas it did not in Fe-FER, all sites active for decomposition in Fe-FER were introduced at low Fe-exchange, whereas in Fe-MOR some other active sites were introduced in high-loaded sample. However, on both systems the activity for N_2O decomposition was markedly lower than that for N_2O reduction with CH_4 (Fig. 7). This result suggests that N_2O decomposition is a demanding reaction occurring only on peculiar sites significantly affected by the topology, whereas the N_2O abatement with CH_4, deleting the difference between the two Fe-zeolites, resulted a facile reaction, occurring on sites that did not (CR_{N2O}) or scarcely (SCR_{N2O}) depended on the topology.

3.3.2.1. N_2O decomposition in hydrothermal conditions. On both Fe-FER-70 and Fe-MOR-95 catalysts, we also investigated the activity, stability and reversibility for N_2O decomposition after addition of water vapor to the feed. On both catalysts, the activity markedly decreased after addition of water vapor to the feed in the whole temperature range (Fig. 8a and c). In particular, at a set temperature the N_2O conversion decreased after H_2O addition, remaining quite stable as a function of time on stream (Fig. 8b and d), suggesting that only a fraction of the active sites was poisoned. After removing H_2O from the feed, the catalysts had to be treated in flow mixture at 500 °C for more than 3 h in order to restore the activity (Fig. 8b and d).

Although on both Fe-FER-70 and Fe-MOR-95 catalysts the inhibiting

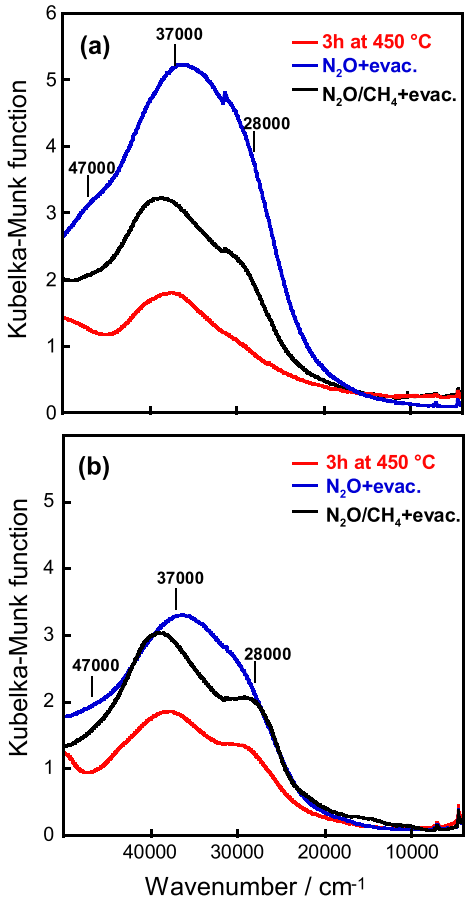

Fig. 9. UV–vis spectra of Fe-MOR-23 (Section a) and Fe-FER-32 (Section b) recorded after the following treatments: 3 h evacuation at 450 °C (red lines), subsequent 5 min interaction with N_2O and evacuation at 250 °C (blue lines) and subsequent 5 min interaction with CH_4 and evacuation at 250 °C (black lines).

effect of water vapor was reversible, the restoring of active sites was dramatically slower for N_2O decomposition than for SCR_{N2O}. This result suggests that the deactivation by H_2O for N_2O decomposition was not due to a reversible H_2O adsorption/desorption phenomenon, but it could be ascribed to a dissociative chemisorption of H_2O on the active sites that required an activated process for H_2O recombination and desorption.

3.4. *In situ UV–vis reactivity study*

The *in situ* UV–vis experiments on thermally activated Fe-MOR-23 and Fe-FER-32 samples (Fig. 9) were focused on the analysis of the changes in the Fe(III) fraction under conditions similar to those occurring during the N_2O decomposition and CR_{N2O}. The aim was to have an insight into the reactivity of $Fe(II)_{ACT}$ species in the N_2O atmosphere and the stability of the Fe(III)-oxo species under CH_4 atmosphere. As the UV–vis spectra recorded in the presence of reactants (N_2O and CH_4) were similar to those recorded after their evacuation, the former spectra were presented in Supplementary Materials (Supplementary Materials, Fig. S9).

The *in situ* UV–vis spectra of thermally activated Fe-MOR-23 and Fe-FER-32 samples (Fig. 9) slightly differed from those of hydrated samples (see Fig. 2), due to the removal of water molecules in the activation process that leads to some coordination changes of Fe species. However, as in hydrated samples, in the spectra of activated samples the bands of isolated Fe(III)Oh/Td species (30,000–50,000 cm^{-1} with a maximum at 37,000 cm^{-1}) and those of di/poly-nuclear Fe(III) species (22,000–30,000 cm^{-1} with main component at about 28,000 cm^{-1}) predominated, while the absence of the band below 18,000 cm^{-1} confirmed the absence of iron oxides in the samples [17,51,53,67]. The population of isolated Fe(III) species in both samples was similar, whereas the fraction of di/poly-nuclear Fe(III) species was lower in Fe-MOR-23 than in Fe-FER-32 sample. Because of the same preparation method and similar iron loading, the UV–vis spectroscopy results indicated that the matrix topology plays a role in the speciation of iron species.

The interaction of Fe-MOR-23 and Fe-FER-32 with N_2O at 250 °C (Supplementary Materials, Fig. S9) followed by desorption (Fig. 9) resulted in the increase of the band intensity in the 30,000–50,000 cm^{-1} and 22,000–30,000 cm^{-1} regions in comparison with those in the activated samples, thus revealing a higher population of either isolated Fe(III) and di/poly-nuclear bridging Fe(III)-oxo species [53]. As was previously shown [3,6,14,23,24,68–70], the interaction of N_2O with Fe(II) in zeolites results in the formation of Fe(III)-O* species able to proceed in the decomposition mechanism towards O_2 desorption. The intensity increase of all the bands typical for Fe(III) after interaction with N_2O suggests that thermally activated samples contained $Fe(II)_{ACT}$ species able to be oxidized by N_2O forming Fe(III)-oxo species (isolated, di/poly-nuclear, and Fe(III)-O* species). These Fe(III)-oxo species were more abundant over Fe-MOR-23 than Fe-FER-32, suggesting a higher stability of the Fe(III)-O* complex in Fe-MOR-23. Taking into account that the N_2O decomposition activity was higher on Fe-FER-32 than on Fe-MOR-23 (see Fig. 7a), the UV–vis results agreed with the literature suggestion that the rate-determining step of N_2O decomposition is the O_2 desorption. As a matter of fact, this step requires the breaking of Fe(III)-O* complex that, being more reactive, resulted in a lower amount in Fe-FER-32 spectrum.

The subsequent heating in CH_4 at 250 °C of Fe-MOR-23 and Fe-FER-32 samples treated with N_2O, mimicking the CR_{N2O} with methane, caused the intensity decrease of the bands of isolated Fe(III) (about 37,000 cm^{-1}) and di/poly-nuclear Fe(III)-oxo species (about 28,000 cm^{-1}) formed after N_2O interactions (Fig. 9), thus suggesting that all these Fe(III)-oxo species were involved in a reduction process by CH_4. The amount of Fe(III)-oxo species formed and stable under N_2O thermal treatment was much higher on Fe-MOR-23 and the amount of residual Fe(III)-oxo species after CH_4 treatment was similar in both samples. It is evident that CH_4 is able to reduce the Fe(III)-oxo species in both zeolites, irrespective of their specific stability induced by the different topology. The similar final population of Fe(III) species after N_2O/CH_4 treatments in the Fe-MOR-23 and Fe-FER-32 catalysts pointed to a similar reactivity of the iron species in the catalytic cycle in the two samples, in agreement with catalytic results for CR_{N2O} (see Fig. 7a). Therefore, these *in situ* UV–vis experiments suggest that the catalytic cycle of CR_{N2O} involved the Fe(II)/Fe(III)-oxo redox cycle in which N_2O activation occurred on a Fe(II) sites forming Fe(III)-oxo species and CH_4 oxidation occurred on the Fe(III)-oxo species restoring the Fe(II) sites. However, under N_2O decomposition conditions only a small fraction of Fe(III)-oxo species, the most reducible one, guaranteed the redox cycle, while in the presence of CH_4 all or a large fraction of Fe(III)-oxo became reactive, due to a levelling effect of CH_4 that made easier the restoring of $Fe(II)_{ACT}$ sites.

3.5. *Operando FTIR study of N_2O reduction in the absence or in the presence of O_2*

Operando FTIR experiments were performed in order to get information on the pathways of CR_{N2O} and SCR_{N2O} and on the key intermediates involved in those processes. The evolution of the surface species formed on the catalysts in the presence of flowing reactant mixtures was inspected as a function of temperature at steady-state conditions or as a function of time by changing the feed composition.

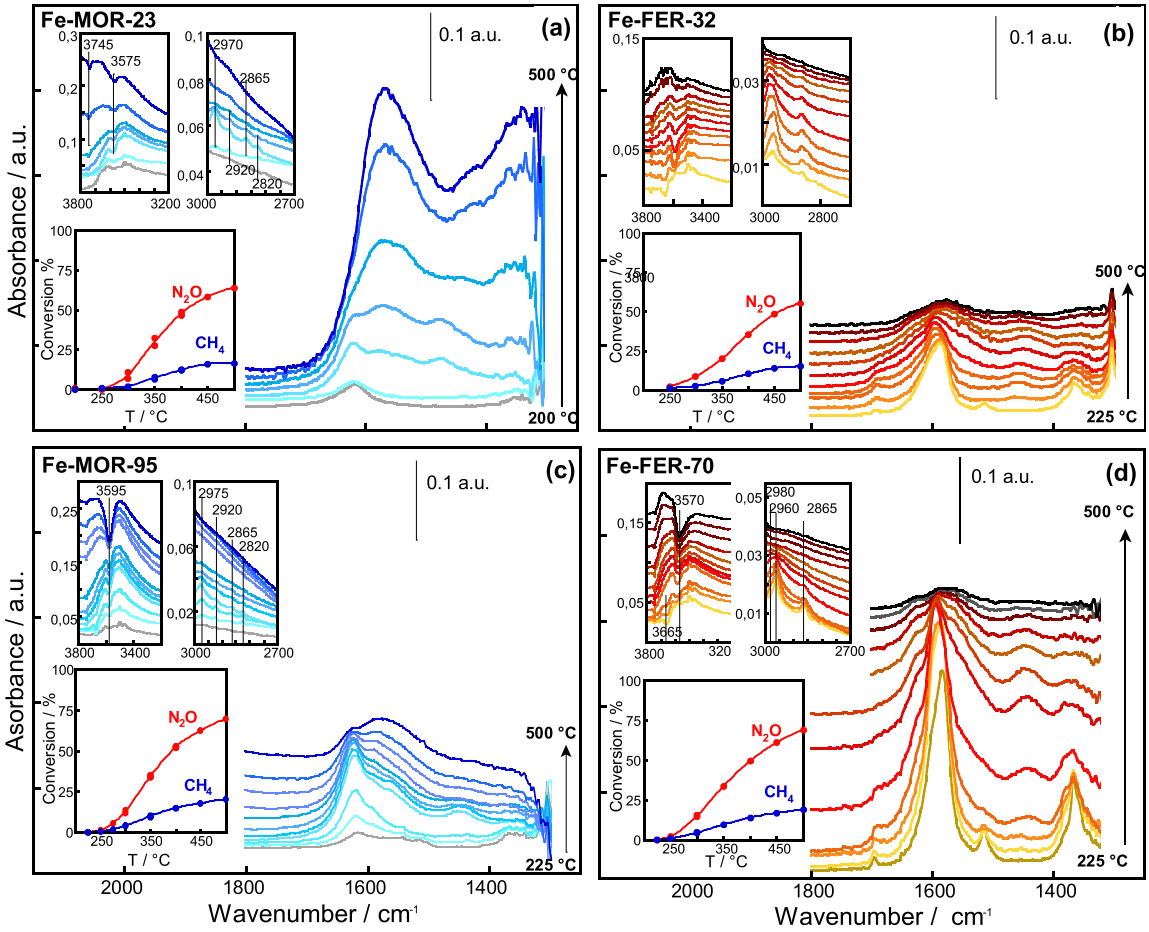

Fig. 10. *Operando* FTIR spectra of surface species during CR_{N2O} reaction at increasing temperature up to 500 °C, stepwise of 50 (Section a) or 25 °C (Sections b,c and d) on Fe-MOR (Sections a and c) and Fe-FER (Sections b and d) catalysts. In the insets, the corresponding reactant conversions as a function of temperature and the magnification of the O-H and C-H stretching region are reported. Reactant concentration: $[N_2O]= [CH_4]= 0.4$ % (total flow rate = 50 cm^3 STP/min, He as balance).

3.5.1. *Steady-state kinetic experiments*

The spectra of Fe-MOR and Fe-FER catalysts under N_2O+CH_4 feed, recorded at increasing temperature in the range (250–400 °C) at which a significant CR_{N2O} activity occurred (Fig. 10 and insets), showed gaseous reactant bands (3016 and 1304 cm^{-1} for CH_4 and at 2223 cm^{-1} for N_2O) and absorptions in the 1700–1300 cm^{-1} and in the 3800–3000 cm^{-1} regions. The absorptions in the 1700–1300 cm^{-1} region could arise from adsorbed incipient H_2O (δ_{H2O} mode at 1625 cm^{-1}) and from various adsorbed CH_xO_y species, the latter in agreement with the weak absorptions of ν_{CH} growing in the 3000–2750 cm^{-1} region (see insets in Fig. 10). Specifically, the bands at about 1650–1600 cm^{-1} could be assigned to both the δ_{H2O} mode of incipient H_2O and to the $\nu_{(C=O)}$ mode of adsorbed formaldehyde-like species (1750–1600 cm^{-1}, depending on the interaction strength of the C=O—surface bond); the complex band at 1590–1560 cm^{-1} and the weak absorptions at 1390 and 1375–45 cm^{-1} could be attributed to $\nu_{as(COO)}$, $\delta_{(CH)}$ and $\nu_{s(COO)}$ of various formate species, while the broad band at 1460 cm^{-1} with the shoulder at 1435 cm^{-1} could be ascribed to $\delta_{as(CH3)}$ and $\delta_{s(CH3)}$ of methoxy species [32,71,72]. These CH_xO_y species arose from the consecutive oxidative dehydrogenation of methane, and were similar to those detected during the methanol oxidation on oxide surfaces [71]. In the OH stretching region (3800–3000 cm^{-1}), spectra showed (i) negative peaks at about 3660 and 3570 cm^{-1} assigned to Fe-OH or semi-extraframework Al-OH species and to Brønsted acid -OH, respectively [73–75] and (ii) a broad absorption at a lower frequency, due to H-bonding interaction of the -OH with adsorbed surface species. On both Fe-FER and Fe-MOR systems, the contemporary CH_4 oxidation, the -OH consumption and H_2O formation suggest a complex active site for CR_{N2O} with two cooperating species yielding a bifunctional pathway: a reactive Fe(III)-oxo species responsible for CH_4 oxidation and an -OH species responsible for the H-extraction.

Comparing FTIR spectra of Fe-FER with Fe-MOR zeolites, in Fe-FER, the CH_xO_y bands were better defined than in Fe-MOR and occurred at a slightly different wavenumber (compare Fig. 10b and d with 10a and c), indicating a lower heterogeneity of surface species and a different interaction with the surface sites depending on the different topology of the matrix. In Fe-FER formate species (1585 cm^{-1}) and formaldehyde-like species (shoulder at 1600 cm^{-1}) were already present in a high amount at 225 °C, below the light-off temperature, indicating that CH_4 was activated at a lower temperature than in Fe-MOR. Above 400 °C, in Fe-MOR a spectral baseline deformation appeared, suggesting coke deposition on the surface, whereas in Fe-FER no coke deposition occurred. Additionally, in Fe-MOR (Fig. 10a and c), broad bands at 1550 and 1350 cm^{-1}, due to formates or carbonate/bicarbonate species [76], prevailed in the spectra. The amount of these latter species was markedly higher in Fe-MOR-23 than in Fe-MOR-95, suggesting that they formed probably involving the OH sites of the MOR matrix whose amount is higher in low-loaded sample. Since in the 350–500 °C temperature range the CH_xO_y bands in the 1630–1350 cm^{-1} region were markedly more intense and more heterogeneous in Fe-MOR-23 than in Fe-FER-32, whereas their activity was similar (see insets of Fig. 10a and b), this intense absorption in Fe-MOR included, besides intermediates, spectator species.

Under $N_2O+CH_4+O_2$ feed, the *operando* FTIR spectra of Fe-MOR and

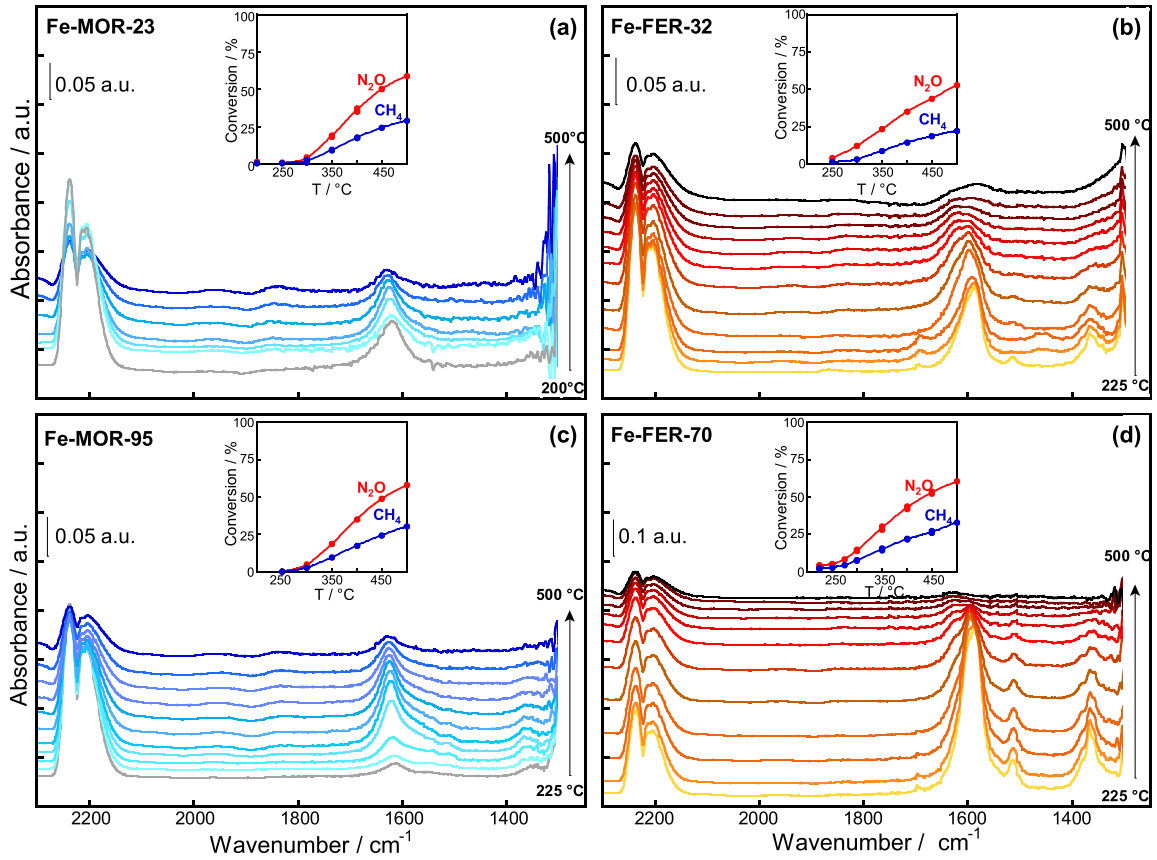

Fig. 11. *Operando* FTIR spectra of surface species during SCR_{N2O} reaction at increasing temperatures up to 500 °C, stepwise of 50 (Section a) or 25 °C (Sections b,c and d) on Fe-MOR (Sections a and c) and Fe-FER (Sections b and d) catalysts. In the inset, the corresponding reactant conversions as a function of temperature are reported. Reactant concentration: $[N_2O]=[CH_4]=0.4$ %, $[O_2]=2$ % (total flow rate = 50 cm^3 STP/min, He as balance).

Fe-FER catalysts at the light-off temperature of SCR_{N2O} (250 °C) showed as main features of the formation of incipient water and of the same CH_xO_y species already observed under N_2O+CH_4 feed, arising from CH_4 activation (Fig. 11). Since these species did not form under CH_4+O_2 feed at increasing temperature (spectra not shown) and all catalysts were inactive for combustion up to 400 °C (see Fig. S8a), in $N_2O+CH_4+O_2$ feed CH_4 reacted more easily with N_2O than with O_2 (confirming suggestion in Section 3.3.2). These findings clearly indicated that, as in CR_{N2O}, also in SCR_{N2O} the first steps of the reaction pathway consisted of N_2O activation and CH_4 oxidative dehydrogenation, whereas O_2 participated in subsequent oxidative steps of CH_xO_y species. In both systems, at increasing temperatures up to 500 °C the amount of adsorbed species decreased.

In Fe-FER samples the amount of the surface CH_xO_y species in $N_2O+CH_4+O_2$ feed was similar to that in N_2O+CH_4 feed, whereas in Fe-MOR zeolites the amount of these species was lower in $N_2O+CH_4+O_2$ feed. This result evidenced the additional effect of O_2 in Fe-MOR samples to prevent the formation of the C-containing species including spectators (1630–1350 cm^{-1} region) and coke.

3.5.2. *Transient kinetic experiments*

To gain further information on the reaction pathway, we added N_2O and CH_4 one by one to the reactant feed at the light-off temperature, changing the addition order, and we investigated the surface species in transient conditions as a function of time on stream. On Fe-MOR-95, the formation of formate and formaldehyde-like intermediates (1550–1650 cm^{-1}) was faster adding N_2O on a surface pre-saturated with CH_4 than adding CH_4 on a surface pre-saturated with N_2O (Fig. 12c, compare spectra at 3 and 7 min). On Fe-FER-70 this trend was observed for the formate at 1585 cm^{-1} alone (Fig. 12d, compare spectra at 3 and 5 min). In parallel with these trends, on both catalysts in the case of pre-saturation with CH_4 (CH_4+N_2O) the activity (ppm of N_2 produced) reached the steady state (constant ppm of N_2 produced, as a function of reaction time) in a lower time than in the case of pre-saturation with N_2O (N_2O+CH_4) (10 vs 17′ on Fe-MOR-95 and 10′ vs 13′ on Fe-FER-70, insets in Fig. 12). These results suggest that formate (band at 1585 cm^{-1}) and formaldehyde-like species formed on Fe-FER zeolite are intermediate species of the N_2O+CH_4 reaction. The faster kinetics to reach the steady-state obtained after pre-saturation with CH_4 suggests that CH_4 reduced some additional Fe(III)-oxo species, still present in the catalysts after the preparation procedure, to $Fe(II)_{RED}$ thus increasing the amount of Fe(II) working sites. Differently, after pre-saturation with N_2O, the same amount of Fe(II) working sites was formed after the addition of CH_4 but in a longer time, because under N_2O flow all the working sites were in the oxidised form. This time was even longer on Fe-MOR-95 than on Fe-FER-70, suggesting that the Fe(III) species reducible with CH_4 were in higher amount in Fe-MOR than in Fe-FER.

In low-loaded Fe-MOR-23, the change of addition order of N_2O and CH_4 in the mixture caused a negligible difference in the kinetics of intermediate formation and of steady-state achievement (Fig. 12a). Differently, in low-loaded Fe-FER-32 the kinetics of intermediate formation and achievement of steady-state was faster by pre-saturating with N_2O (Fig. 12b). These findings were probably due to the fact that the amount of Fe(III)-oxo species that underwent reduction in CH_4 feed was in a small amount in low-loaded Fe-MOR-23, and in a negligible amount in low-loaded Fe-FER-32, where all Fe(II) active sites were already present after activation, as suggested by *in situ* FTIR spectra after

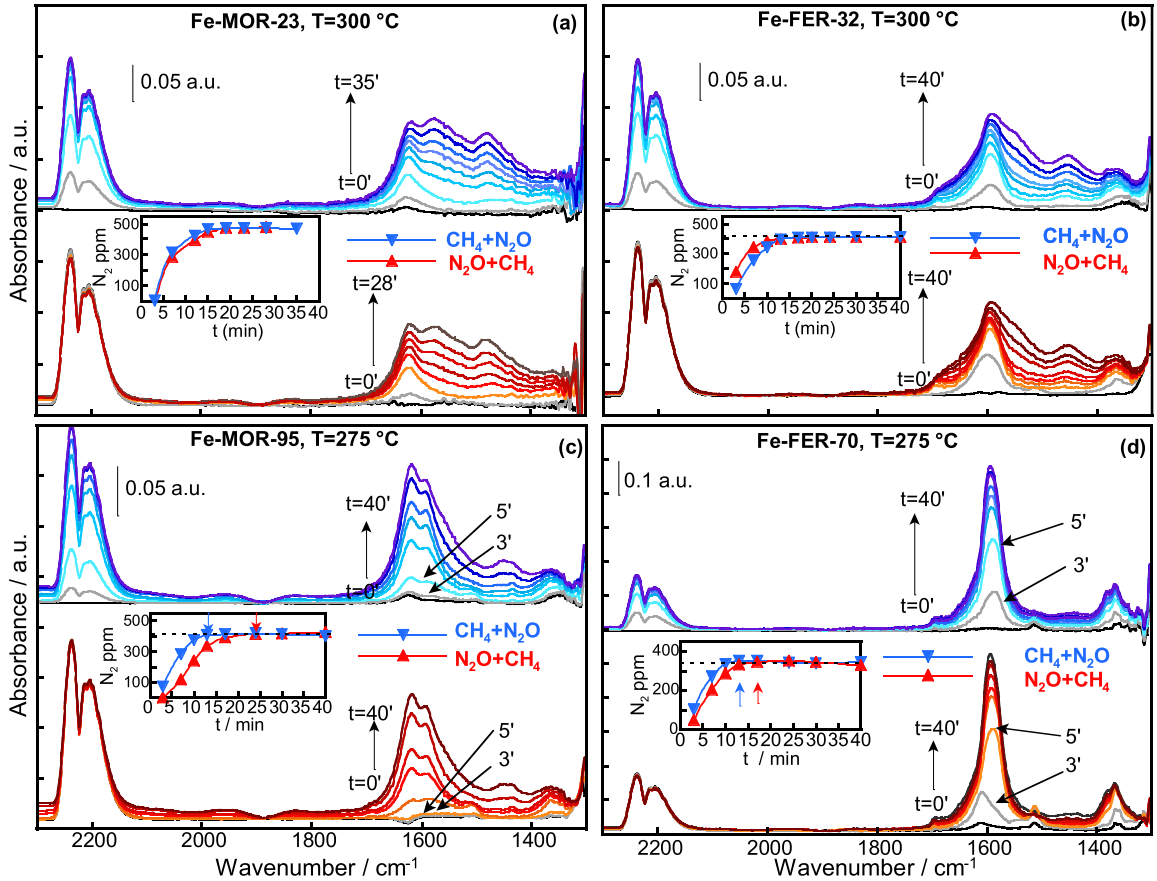

Fig. 12. The surface species formed on the Fe-MOR (Sections a and b) and Fe-FER catalysts (Sections c and d) after addition to the reactant feed of N_2O and CH_4 one by one, changing the addition order, at increasing mixing time and at a constant temperature (as indicated). The FTIR spectra were recorded after pre-saturating the surface with the first reactant (t = 0′, black lines) and at increasing time after the subsequent addition of the second reactant (N_2O+CH_4 or CH_4+N_2O, as specified). In the insets, the corresponding N_2 ppm produced as a function of time is depicted. Reactant concentration: [N_2O]= [CH_4]= 0.4 % (total flow rate=50 cm^3 STP/min, He as balance).

reductant thermal treatment in CO.

In Fe-MOR samples and in low-loaded Fe-FER-32, when the catalytic activity reached the steady state, the amount of some surface species in the 1630–1350 cm^{-1} region continued to slightly grow with reaction time, reinforcing the hypothesis that some of these species were spectator species.

The subsequent addition of O_2 to the N_2O+CH_4 feed at the same temperature on Fe-FER-32 did not affect both the activity at the steady-state and the band intensity of formate at 1585 cm^{-1} and formaldehyde, while the formate at 1560 cm^{-1} and methoxy bands progressively disappeared (Fig. 13a and b). Therefore, these latter species were only spectators, whereas the former were possible intermediates. Differently, on Fe-MOR-23, the O_2 addition caused a fast decrease of the activity and a small decrease of the band intensity of surface CH_xO_y species at 1610–1585 cm^{-1}, while the bands of methoxy and formate at 1560 cm^{-1} continued to decrease, almost disappearing when the activity has reached the SCR_{N2O} steady-state (Fig. 13c and d). This confirmed that the latter species were spectators, whereas the former species were possible intermediates.

The addition of O_2 to the CR_{N2O} feed (SCR_{N2O}), leaving unchanged the activity of Fe-FER whereas lowering that of Fe-MOR, indicated that in Fe-MOR O_2 affected a parameter crucial for the reaction, such as the pathway, the amount and/or type of intermediates, and the amount of active sites. We can exclude a negative effect of O_2 on the reaction pathway, because the stoichiometry (N_2O/CH_4 and O_2/CH_4 ratios, see Fig. S7), the CO_2 selectivity and the apparent activation energy values (see Fig. 5) in Fe-MOR were similar to those in Fe-FER series. We can also exclude a negative effect of O_2 on the nature of intermediates because they were the same in both CR_{N2O} and SCR_{N2O} (formate at 1585 cm^{-1} and adsorbed formaldehyde species). Since in Fe-MOR the addition of O_2 lowered the concentration of these intermediates and the activity, we suggest that a small fraction of the $Fe(II)_{RED}$ species (the least stable ones of those formed by CH_4) was re-oxidised by O_2, thus decreasing the amount of Fe(II) working sites for SCR_{N2O}.

On the whole, considering that after the thermal activation $Fe(II)_{ACT}$ and Fe(III)-oxo species coexisted in Fe-MOR and Fe-FER catalysts, the CR_{N2O} reaction pathway might start (i) on $Fe(II)_{ACT}$ sites with the activation of N_2O yielding reactive Fe(III)-O* species that is a part of the bifunctional active sites on which CH_4 activation takes place, and (ii) on Fe(III)-oxo species reducible by CH_4 yielding $Fe(II)_{RED}$ on which N_2O activation takes place. The formation of CH_xO_y surface species is the result of the contemporary activation of N_2O and CH_4.

3.5.3. *Operando FTIR study of SCR_{N2O} in the presence of H_2O*

On both Fe-FER-70 and Fe-MOR-95 catalysts *operando* FTIR experiments at decreasing temperature confirmed the catalytic results obtained in the plug-flow reactor (see Fig. 6) showing that the activity for SCR_{N2O} in the presence of H_2O (N_2O+CH_4+O_2+H_2O feed) was lower than that in the absence of H_2O in the whole temperature range (500–225 °C, insets in Fig. 14).

The spectra at the highest temperature (500 °C) in both experiments (with or without H_2O in the feed) showed only the bands of incipient adsorbed H_2O (δ_{HOH} at 1625 cm^{-1} and broad absorption of H-bonded OH in the 3700–3200 cm^{-1} region) formed as reduction product. On Fe-

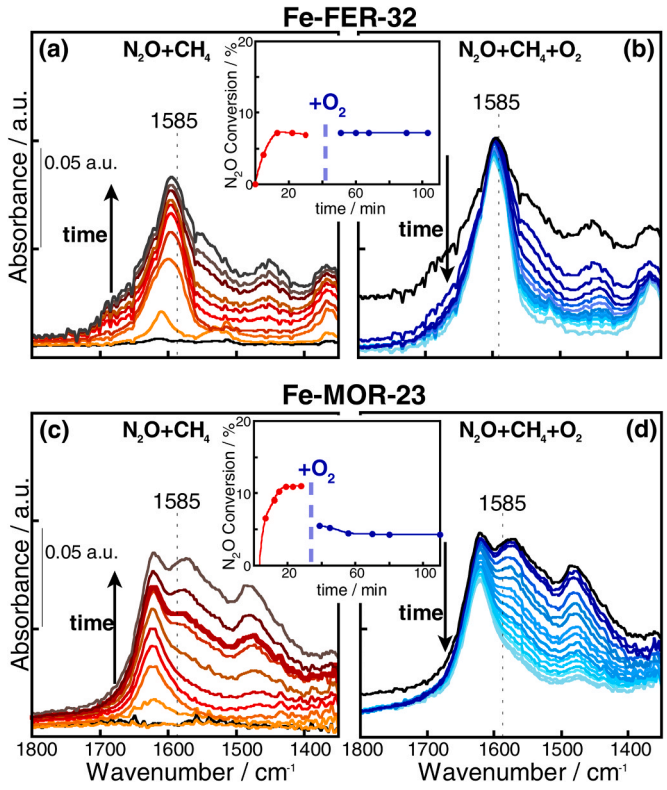

Fig. 13. The surface species formed at a constant temperature (300 °C) and increasing time on the Fe-MOR-23 (Sections a and b) and Fe-FER-32 (Sections c and d) catalysts. Spectra are recorded after pre-saturating the surface with N_2O (t = 0′) and the subsequent addition of the CH_4 (Sections a and c); after the addition of O_2 to the reactant N_2O+CH_4 feed (Sections b and d). In the inset, the corresponding N_2O conversion as a function of time is reported. Reactant concentration: [N_2O]= [CH_4]=0.4 %, [O_2]=2 % (total flow rate=50 cm^3 STP/min, He as balance).

FER-70 at decreasing temperature in the H_2O-containing feed, formate and formaldehyde bands appeared as defined shoulders of the 1625 cm^{-1} band (1585 and 1600 cm^{-1}, respectively), that were markedly less intense than in the feed without H_2O (Fig. 14a). In parallel, the adsorbed H_2O band progressively increased and became prevalent below 300 °C. The hindrance to the formation of formate at 1585 cm^{-1} and formaldehyde species and the parallel activity decrease confirm that these species were intermediates. We followed the evolution in the time of the surface species formed after adding H_2O to the feed at 315 °C, the temperature at which the activity was kinetically significant (about 25% of conversion). In parallel to the N_2O conversion decrease (Fig. 14b), the transient experiments showed the progressive decrease of formate at 1585 cm^{-1} and formaldehyde bands (envelope with a maximum at 1597 cm^{-1}) and the simultaneous increase of adsorbed H_2O band, yielding an isosbestic point at about 1612 cm^{-1} (insets in Fig. 14b). The subsequent elimination of the H_2O from the feed caused the complete reversibility of this trend, reproducing as the intensity of all the bands as the catalytic activity (Fig. 14b).

On Fe-MOR-95, in the presence of H_2O in the feed at decreasing temperature, the change of surface species was similar to that reported for Fe-FER-70, even if less evident in the spectra (Fig. 14c). In fact, the bands of formate at 1585 cm^{-1} and formaldehyde intermediates were not defined and were only deducible by the red-shift of the envelope at 1625 cm^{-1} as the temperature decreased. Also in this case, the transient experiment at constant temperature (350 °C, Fig. 14d) showed that the removal of the water from the feed reversibly restored the initial surface species and their reactivity.

On the whole these results indicate that H_2O deactivated some active sites for SCR_{N2O} *via* a reversible molecular adsorption, saturating their coordination sphere. This suggestion is consistent with the relatively fast recovery of activity observed when H_2O was switched-off (about 50 min, half of which is required to obtain a H_2O-free feeding) corresponding to H_2O desorption.

3.6. *Active sites and reaction pathways for N_2O abatement reactions*

To have an insight into the active sites and reaction pathways of N_2O abatement in Fe-MOR and Fe-FER, we correlated the catalytic results with the *in situ* (FTIR and UV–vis) characterisation and *operando* FTIR results.

For the CR_{N2O} reaction Fe-MOR and Fe-FER catalysts are highly and similarly active. For SCR_{N2O}, Fe-FER samples display the same activity as for CR_{N2O}, whereas Fe-MOR zeolites turned out less active. For N_2O decomposition, all catalysts are markedly less active than for reduction, and Fe-FER showed much higher activity than Fe-MOR series (10 times more, see Fig. S8). For all N_2O abatement reactions, Fe(II) species are generally recognised to be the active sites. In the present study, FTIR and UV–vis characterisation allowed us to distinguish among Fe(II) species having different coordinative unsaturation, because upon NO adsorption they formed either Fe(II)-mononitrosyl or Fe(II)-polynitrosyls. The relative amount Fe(II)-mononitrosyl/Fe(II)-polynitrosyls depended on the zeolite topology (see Fig. S6). In the investigated samples, all Fe(II) species originated from Fe(III)-oxo species, introduced in the preparation, which can be listed in three families characterized by different redox mobility. On both Fe-FER and Fe-MOR systems, the first family of Fe(III)-oxo consists of the most reducible species that give origin to highly stable $Fe(II)_{ACT}$ after thermal activation treatment. The second family of Fe(III)-oxo species is not reducible by thermal activation and requires an additional thermal treatment with a reductant (CO or CH_4) to give Fe(II) species indicated as $Fe(II)_{RED}$ (FTIR evidence, see Section 3.2.2). As it will be shown later, a third family of Fe(III)-oxo is only present on Fe-MOR, and consists of the less reducible species unable to yield Fe(II) active sites under SCR_{N2O} feed.

A fraction of $Fe(II)_{ACT}$ species represent the active sites for N_2O decomposition yielding Fe(III)-O* by N_2O activation. The stability of this Fe(III)-O* species is considered as the main factor affecting the final O_2 desorption step [23–26,68,77]. In addition to what was reported in previous studies [10,12,18,21], also the following considerations suggest that the speciation of $Fe(II)_{ACT}$ is different in FER with respect to MOR. In Fe-FER catalysts the activity for N_2O decomposition is related to the amount of mono-nitrosyl complexes, because at increasing Fe-loading the amount of Fe(II)-polynitrosyls increases but the amount of mono-nitrosyl complexes and the catalytic activity do not (see FTIR spectra in Fig. 3 and N_2O conversion in Fig. S8b). Therefore, only a small fraction of Fe(II), namely the $Fe(II)_{ACT}$ species having less coordinative unsaturation, are active for N_2O decomposition. These active sites are introduced in the early stage of preparation reaching the maximum amount at low iron-loading, as suggested by the evidence that the activity is constant at increasing Fe-loading. Although MOR and FER matrices have in their framework a comparable amount of Al pairs responsible for Fe(II) stabilization, the FER matrix provides favorable structural features for the stabilization of $Fe(II)_{ACT}$ species. As a consequence, N_2O is quickly split into N_2 and adsorbed O* yielding Fe(III)-O*, thanks to the peculiar structure of the binuclear cationic sites [18], and at the same time the Fe(III)-O* intermediate is highly reactive (UV–vis evidence) making faster also the second step (Fe(III)-O* + N_2O → Fe(II) + O_2 + N_2) which is generally rate-determining. In MOR, instead, the $Fe(II)_{ACT}$ species may consist in non-axial binuclear Fe(II) sites, less active than FER active sites [18], and in short-distance Fe(II)-□-Fe(II) dimers as suggested in [30]. In the latter case, the decomposition of N_2O results in the formation of a dimeric Fe^{3+}-$O^{(1+\delta)-}$-$Fe^{(2+\delta)+}$ intermediate, quasi-oxidic in character, which is more stable than Fe(III)-O* in FER and displays a lower reactivity in the second step of the reaction. On both systems, a fraction of $Fe(II)_{ACT}$ species active for N_2O

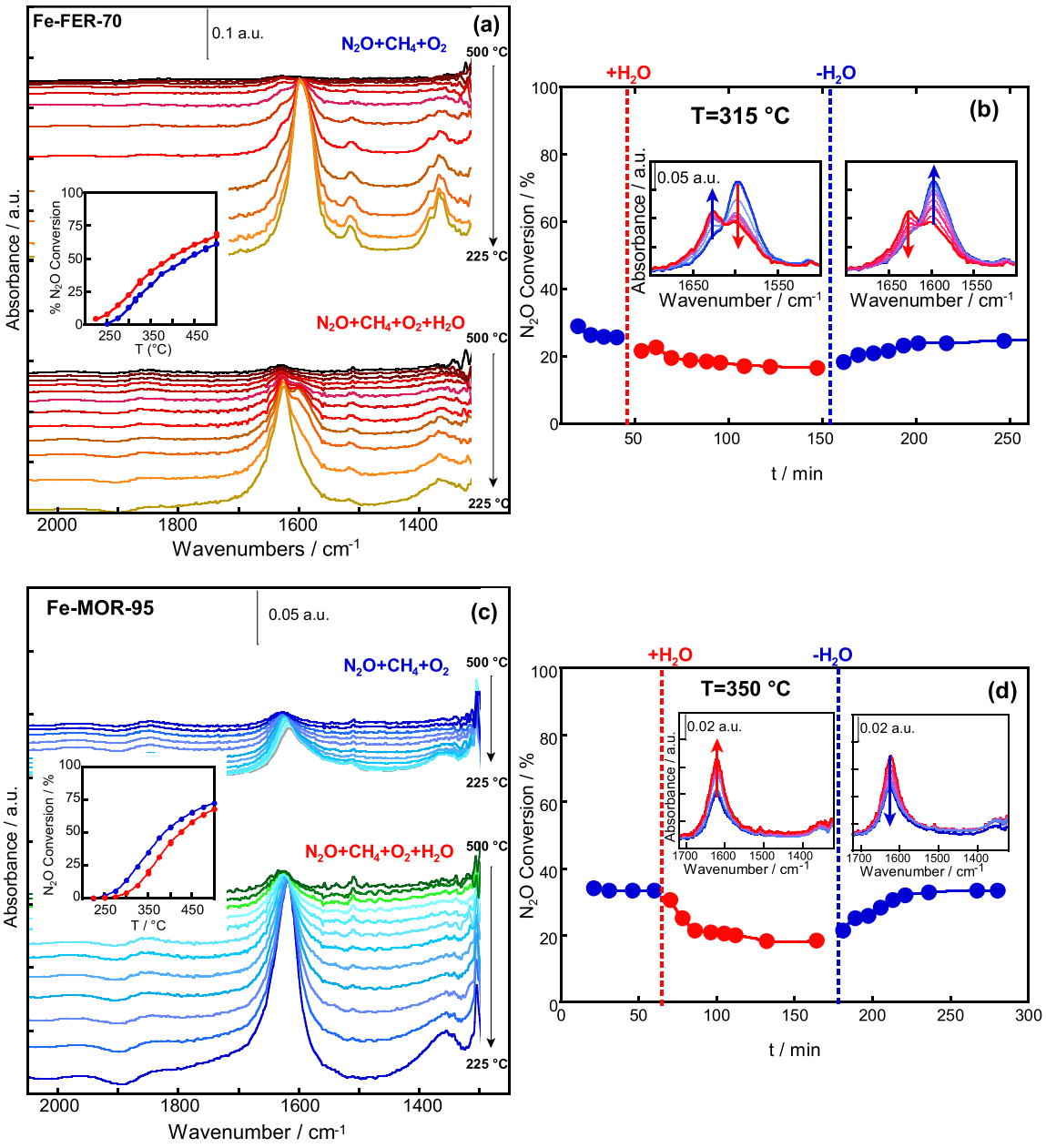

Fig. 14. *Operando* FTIR spectra of surface species during SCR_{N2O} reaction, in the presence or in the absence of H_2O in the feed, on Fe-FER-70 (Sections a and b) and Fe-MOR-95 (Sections c and d) catalysts. Sections a and c: spectra collected at decreasing temperature from 500 to 225°C, stepwise of 25 °C; in the insets, the corresponding N_2O conversion as a function of temperature is reported. Sections b and d: spectra collected at a constant temperature (315 °C for Fe-FER-70, 350 °C for Fe-MOR-95) at increasing contact time before, after addition and after removal of H_2O to the reactant (N_2O+CH_4+O_2) feed; in the insets, the corresponding surface species modification as a function of time. Reactant concentration: [N_2O]= [CH_4]=0.4 %, [O_2]=2 %, [H_2O]=0 or 2 % (total flow rate = 50 cm^3 STP/min, He as balance).

decomposition was deactivated by H_2O. This effect could be ascribed to the transformation of active Fe(II) sites to hydroxylated Fe(III) species *via* oxidation/hydroxylation by N_2O in the presence of water, as already suggested for Fe-ZSM5 catalysts [78]. To restore the Fe(II) active sites a thermally activated reducing/dehydrating treatment was necessary.

With respect to decomposition, the addition of CH_4 to the N_2O feed considerably improved the activity for N_2O abatement. As a matter of fact, methane yielded a higher amount of Fe(II) active sites by reducing additional Fe(III)-oxo to $Fe(II)_{RED}$ species. In high-loaded samples this reduction was evidenced (i) by the increase of Fe(II)-nitrosyl and carbonyl bands after thermal treatment with a reductant (see Fig. 3) and (ii) by the faster kinetics to reach the CR_{N2O} steady-state in CH_4+N_2O mixture when the surface was pre-saturated with CH_4 (see Fig. 12). A second effect of CH_4 was to recover the Fe(II) active sites by reduction of Fe(III)-O* intermediates with a faster process than O_2 desorption in the N_2O decomposition. This suggestion was supported by the values of apparent activation energy, calculated from the data in Fig. 7, lower in CR_{N2O} (81–94 kJ/mol) than in N_2O decomposition (110–138 kJ/mol). In the Fe-FER-32 low-loaded sample, this second effect of CH_4 was predominant because a negligible amount of $Fe(II)_{RED}$ formed (*in situ* FTIR evidence, see Fig. 3) and the pre-saturation of the surface with CH_4 did not favour the CR_{N2O} steady-state achievement (see Fig. 12b).

With respect to CR_{N2O}, the addition of O_2 to the feed (SCR_{N2O}) lowered the activity of Fe-MOR, suggesting that a small fraction of the $Fe(II)_{RED}$ active species was re-oxidised by O_2, thus decreasing the amount of Fe(II) active sites for SCR_{N2O}. This hypothesis is supported by the

evidence that the pre-exponential factor of the Arrhenius equation (y-intercept in the Arrhenius plot, Fig. 5), proportional to the number of active sites, decreases for SCR_{N2O} with respect to CR_{N2O}. Therefore, on MOR a third family of Fe(III)-oxo species could be identified, capable of producing Fe(II) sites under CR_{N2O} conditions which are re-oxidized under SCR_{N2O} conditions. The above Fe(II) species, the less stable among those formed by CH_4, probably belong to dimeric Fe(II)-□-Fe(II) species with a configuration suitable to react with molecular O_2 and to stabilize adducts like peroxidic or bis-μ-oxo species, as suggested for Fe and Cu dimers in zeolites [79,80]. The structure and amount of these peculiar dimeric species seems specific for the MOR topology. Conversely, independently of the zeolite topology, the addition of H_2O to the SCR_{N2O} feed caused a slight and reversible deactivation of Fe-FER and Fe-MOR catalysts, ascribed to H_2O adsorption/desorption phenomena on some iron sites, which are prevented from interacting with the reactants.

With respect to the reaction pathway, *operando* FTIR measurements on CR_{N2O} and SCR_{N2O} detected the formation of CH_xO_y surface species and incipient H_2O, suggesting that the CH_4 oxidative dehydrogenation occurs in the presence of N_2O. In the presence of CH_4+O_2 feed, neither CH_4 combustion occurred below 400 °C nor surface species were observed, indicating that the N_2O reaction with the surface is required to yield the sites able to activate CH_4 in CR_{N2O}. Therefore, we suggest that the reaction pathway occurs on a bifunctional site consisting of a reactive Fe(III)-oxo species for CH_4 oxidation, assisted by a OH species at a close distance for H-extraction. The reactive Fe(III)-oxo species could be (i) the Fe(III)-O* species arising from N_2O activation on bare Fe(II) or (ii) the labile oxygen atoms in Fe(III)-O-Fe(III) dimers (see Section 3.2.1.). As a final remark, *operando* FTIR also showed that, among the CH_xO_y surface species, specific formate (at 1585 cm^{-1}) and formaldehyde are reaction intermediates. In the CR_{N2O} all the above species are further oxidized step by step by N_2O up to the final products (CO_2, H_2O, CO, H_2). In the SCR_{N2O}, stoichiometric ratios indicated that, besides N_2O, also O_2 takes part in these oxidative steps of the pathway (see Fig. S7).

4. Conclusions

In Fe-MOR and Fe-FER zeolites, the matrix topology and Al pairs location affect the speciation of iron species. Although FER and MOR matrices have in their framework a comparable amount of Al pairs, their location, depending on the zeolite topology, determines the formation of Fe(II) species that, differing in the coordinative unsaturation and redox properties, have a different activity for the N_2O abatement reactions. In all Fe-MOR and Fe-FER catalysts the N_2O reduction with CH_4, in the absence or in the presence of O_2 (CR_{N2O} and SCR_{N2O}) is markedly more efficient than the N_2O decomposition. Fe-FER is more active than Fe-MOR for the reduction of N_2O in the presence of O_2 (SCR_{N2O}) and for the N_2O decomposition, whereas both systems are similarly active for CR_{N2O}.

The FER topology offers structural features for the stabilization of peculiar Fe(II) species that are introduced in the early stage of preparation and are more homogeneous and stable with respect to MOR also in the presence of O_2. Among these species, specific couples of bare Fe (II) ions (iron binuclear centers), in spite of a low coordinative unsaturation, easily split N_2O thanks to their specific arrangement, yielding highly reactive Fe(III)-oxo intermediates which are easily reconverted to Fe(II). This accounts for the higher activity for N_2O decomposition of Fe-FER with respect to Fe-MOR. The MOR topology, which does not allow the arrangement of these Fe(II) active species, favors the formation of the Fe(II)-□-Fe(II) species less active for N_2O decomposition.

Both MOR and FER topologies stabilize a bifunctional site active for the CR_{N2O} and SCR_{N2O} reactions, capable to activate N_2O and CH_4. This bifunctional active site consists of peculiar Fe(II) species, forming reactive Fe(III)-oxo by N_2O activation, and of a nearby reactive OH which is involved in the CH_4 oxidative dehydrogenation by H-extraction and H_2O formation. The pathway is accomplished through the formation of surface specific formate (at 1585 cm^{-1}) and formaldehyde species, suggested as reaction intermediates. The O_2 in the feed of SCR_{N2O} takes part in oxidative steps of these intermediates, causing a decrease of the CH_4 efficiency towards N_2O with respect to CR_{N2O}. In the Fe-MOR catalysts, in addition, O_2 has the detrimental effect to poison some Fe(II) active sites. Due to MOR topology, some dimeric Fe(II)-□-Fe(II) species have probably the geometry and Fe-Fe distance suitable to react with molecular O_2, stabilizing non-reactive Fe(III)-oxo species.

In both systems, the addition of H_2O to the SCR_{N2O} feed cause a slight and reversible deactivation due to adsorption/desorption phenomena. However, the limited extent of the interaction with H_2O allows both Fe-FER and Fe-MOR systems to be potentially effective catalysts for N_2O abatement with CH_4 in real conditions, i.e. with oxygen and water vapor in the feed, Fe-FER being more efficient due to its better resistance to the presence of O_2 in the reaction feed.

CRediT authorship contribution statement

M.C.C. - Conceptualization, Catalytic tests, FTIR study, Data analysis, D.P. - Conceptualization, FTIR and UV–vis study, Data analysis, C.C. - FTIR study and data analysis, S.M. – Formal analysis, J.O.- NMR measurement and data analysis, K.M.- Samples preparation, determination of Al distribution, M.L.- Samples preparation, J.D. - NMR study, A.K. – Samples preparation, UV-vis study, E.T.- Conceptualization, samples preparation, in-situ UV–vis measurements, data analysis. All authors participated in the manuscript preparation.

Declaration of Competing Interest

The authors declare that they have no known competing financial interests or personal relationships that could have appeared to influence the work reported in this paper.

Data Availability

Data will be made available on request.

Acknowledgments

This work was supported by the 'Sapienza' University of Rome (Research Project 2019 - Grant n. RM11916B8935A62C), RVO: 61388955, and the Project of International Mobility of Researchers, Technical and Administrative Workers of Research Institutions (MEYS, OP RDE) "Optimalisation of analytical methods for environmental and biomedical diagnostics", Reg.No. Cz.02.2.69/0.0/0.0/18_053/0016922, Key Activity: Redox Catalysts for Environmental Processes II. Authors wish to thank Prof. Manlio Occhiuzzi for the useful discussion on the result interpretation.

Appendix A. Supporting information

Supplementary data associated with this article can be found in the online version at doi:10.1016/j.apcatb.2023.123360.

References

[1] M. Konsolakis, Recent advances on nitrous oxide (N_2O) decomposition over non-noble-metal oxide catalysts: catalytic performance, mechanistic considerations, and surface chemistry aspects, ACS Catal. 5 (2015) 6397–6421, https://doi.org/10.1021/acscatal.5b01605.

[2] ⟨https://op.europa.eu/en/publication-detail/-/publication/ed0fcc33–1283-11e6-ba9a-01aa75ed71a1⟩.

[3] M.L. Bols, B.E.R. Snyder, H.M. Rhoda, P. Cnudde, G. Fayad, R.A. Schoonheydt, V. Van Speybroeck, E.I. Solomon, B.F. Sels, Coordination and activation of nitrous oxide by iron zeolites, Nat. Catal. 4 (2021) 332–340, https://doi.org/10.1038/s41929-021-00602-4.

[4] M.C. Campa, V. Indovina, D. Pietrogiacomi, The dependence of catalytic activity for N2O decomposition on the exchange extent of cobalt or copper in Na-MOR, H-

MOR and Na-MFI, Appl. Catal. B-Environ. 91 (2009) 347–354, https://doi.org/10.1016/j.apcatb.2009.05.042.
[5] D. Pietrogiacomi, M.C. Campa, M. Occhiuzzi, Selective catalytic reduction of N2O with CH4 on Ni-MOR: A comparison with Co-MOR and Fe-MOR catalysts, Catal. Today 227 (2014) 116–122, https://doi.org/10.1016/j.cattod.2013.09.014.
[6] P.J. Smeets, J.S. Woertink, B.F. Sels, E.I. Solomon, R.A. Schoonheydt, Transition-metal ions in zeolites: coordination and activation of oxygen, Inorg. Chem. 49 (2010) 3573–3583, https://doi.org/10.1021/ic901814f.
[7] ⟨https://d2zo35mdb530wx.cloudfront.net/_legacy/UCPthyssenkruppBAIS/assets.files/products__services/fertilizer_plants/nitrate_plants/brochure-envinox_scr.pdf⟩.
[8] J. Dedecek, Z. Sobalik, B. Wichterlova, Siting and distribution of framework aluminium atoms in silicon-rich zeolites and impact on catalysis, Catal. Rev. -Sci. Eng. 54 (2012) 135–223, https://doi.org/10.1080/01614940.2012.632662.
[9] J. Dedecek, E. Tabor, S. Sklenak, Tuning the aluminum distribution in zeolites to increase their performance in acid-catalyzed reactions, ChemSusChem 12 (2019) 556–576, https://doi.org/10.1002/cssc.201801959.
[10] Z. Sobalik, J. Novakova, J. Dedecek, N.K. Sathu, E. Tabor, P. Sazama, P. Stastny, B. Wichterlova, Tailoring of Fe-ferrierite for N_2O decomposition: on the decisive role of framework Al distribution for catalytic activity of Fe species in Fe-ferrierite, Microporous Mesoporous Mater. 146 (2011) 172–183, https://doi.org/10.1016/j.micromeso.2011.05.004.
[11] L. Kiwi-Minsker, D.A. Bulushev, A. Renken, Active sites in HZSM-5 with low Fe content for the formation of surface oxygen by decomposing N_2O: Is every deposited oxygen active? J. Catal. 219 (2003) 273–285, https://doi.org/10.1016/s0021-9517(03)00222-7.
[12] K. Jisa, J. Novakova, M. Schwarze, A. Vondrova, S. Sklenak, Z. Sobalik, Role of the Fe-zeolite structure and iron state in the N2O decomposition: comparison of Fe-FER, Fe-BEA, and Fe-MFI catalysts, J. Catal. 262 (2009) 27–34, https://doi.org/10.1016/j.jcat.2008.11.025.
[13] M. Lemishka, J. Dedecek, K. Mlekodaj, Z. Sobalik, S. Sklenak, E. Tabor, Speciation and siting of divalent transition metal ions in silicon-rich zeolites. An FTIR study, Pure Appl. Chem. 91 (2019) 1721–1732, https://doi.org/10.1515/pac-2018-1228.
[14] I. Melian-Cabrera, C. Mentruit, J.A.Z. Pieterse, R.W. van den Brink, G. Mul, F. Kapteijn, J.A. Moulijn, Highly active and stable ion-exchanged Fe-Ferrierite catalyst for N2O decomposition under nitric acid tail gas conditions, Catal. Commun. 6 (2005) 301–305, https://doi.org/10.1016/j.catcom.2005.01.004.
[15] H. Guesmi, D. Berthomieu, L. Kiwi-Minsker, Nitrous oxide decomposition on the binuclear Fe-II(mu-O)(mu-OH)Fe-II center in Fe-ZSM-5 zeolite, J. Phys. Chem. C 112 (2008) 20319–20328, https://doi.org/10.1021/jp808044r.
[16] D.A. Bulushev, P.M. Prechtl, A. Renken, L. Kiwi-Minsker, Water vapor effects in N_2O decomposition over Fe-ZSM-5 catalysts with low iron content, Ind. Eng. Chem. Res. 46 (2007) 4178–4185, https://doi.org/10.1021/ie061134.
[17] L. Čapek, V. Kreibich, J. Dědeček, T. Grygar, B. Wichterlová, Z. Sobalík, J. A. Martens, R. Brosius, V. Tokarová, Analysis of Fe species in zeolites by UV–VIS–NIR, IR spectra and voltammetry. Effect of preparation, Fe loading and zeolite type, Microporous Mesoporous Mater. 80 (2005) 279–289, https://doi.org/10.1016/j.micromeso.2004.12.014.
[18] E. Tabor, M. Lemishka, J.E. Olszowka, K. Mlekodaj, J. Dedecek, P. C. Andrikopoulos, S. Sklenak, Splitting dioxygen over distant binuclear Fe sites in zeolites. Effect of the local arrangement and framework topology, ACS Catal. 11 (2021) 2340–2355, https://doi.org/10.1021/acscatal.0c04459.
[19] E. Tabor, G. Sádovská, M. Bernauer, P. Sazama, J. Nováková, V. Fíla, T. Kmječ, J. Kohout, K. Závěta, Z. Sobalík, Feasibility of application of iron zeolites for high-temperature decomposition of N_2O under real conditions of the technology for nitric acid production, Appl. Catal. B-Environ. 240 (2019) 358–366, https://doi.org/10.1016/j.apcatb.2017.11.014.
[20] S. Sklenak, P.C. Andrikopoulos, B. Boekfa, B. Jansang, J. Novakova, L. Benco, T. Bucko, J. Hafner, J. Dedecek, Z. Sobalik, N_2O decomposition over Fe-zeolites: structure of the active sites and the origin of the distinct reactivity of Fe-ferrierite, Fe-ZSM-5, and Fe-beta. A combined periodic DFT and multispectral study, J. Catal. 272 (2010) 262–274, https://doi.org/10.1016/j.jcat.2010.04.008.
[21] E. Tabor, J. Dedecek, K. Mlekodaj, Z. Sobalik, P.C. Andrikopoulos, S. Sklenak, Dioxygen dissociation over man-made system at room temperature to form the active α-oxygen for methane oxidation, eaaz9776, Sci. Adv. 6 (2020), https://doi.org/10.1126/sciadv.aaz9776.
[22] K. Mlekodaj, M. Lemishka, A. Kornas, D.K. Wierzbicki, J.E. Olszowka, H. Jirglová, J. Dedecek, E. Tabor, Evolution of active oxygen species originating from O_2 cleavage over Fe-FER for application in methane oxidation, ACS Catal. 13 (2023) 3345–3355, https://doi.org/10.1021/acscatal.2c06099.
[23] D. Pietrogiacomi, M.C. Campa, L.R. Carbone, M. Occhiuzzi, N_2O decomposition and reduction on Co-MOR, Fe-MOR and Ni-MOR catalysts: in situ UV–vis DRS and operando FTIR investigation. An insight on the reaction pathways, Appl. Catal. B-Environ. 240 (2019) 19–29, https://doi.org/10.1016/j.apcatb.2018.08.046.
[24] F. Kapteijn, J. Rodriguez Mirasol, J.A. Moulijn, Heterogeneous catalytic decomposition of nitrous oxide, Appl. Catal. B-Environ. 9 (1996) 25–64, https://doi.org/10.1016/0926-3373(96)90072-7.
[25] F. Kapteijn, G. Marbán, J. Rodriguez-Mirasol, J.A. Moulijn, Kinetic analysis of the decomposition of nitrous oxide over ZSM-5 catalysts, J. Catal. 167 (1997) 256–265, https://doi.org/10.1006/jcat.1997.1581.
[26] Y. Li, J.N. Armor, Catalytic decomposition of nitrous oxide on metal exchanged zeolites, Appl. Catal. B-Environ. 1 (1992) L21–L29, https://doi.org/10.1016/0926-3373(92)80019-V.
[27] A. Zecchina, M. Rivallan, G. Berlier, C. Lamberti, G. Ricchiardi, Structure and nuclearity of active sites in Fe-zeolites: comparison with iron sites in enzymes and homogeneous catalysts, Phys. Chem. Chem. Phys. 9 (2007) 3483–3499, https://doi.org/10.1039/b703445h.
[28] K.A. Dubkov, N.S. Ovanesyan, A.A. Shteinman, E.V. Starokon, G.I. Panov, Evolution of iron states and formation of α-sites upon activation of FeZSM-5 zeolites, J. Catal. 207 (2002) 341–352, https://doi.org/10.1006/jcat.2002.3552.
[29] M.L. Bols, H.M. Rhoda, B.E.R. Snyder, E.I. Solomon, K. Pierloot, R.A. Schoonheydt, B.F. Sels, Advances in the synthesis, characterisation, and mechanistic understanding of active sites in Fezeolites for redox catalysts, Dalton Trans. 49 (2020) 14749–14757, https://doi.org/10.1039/d0dt01857k.
[30] M.C.E. Groves, A. Sasonow, Uhde EnviNO$_x$® technology for NO_x and N_2O abatement: a contribution to reducing emissions from nitric acid plants, J. Integr. Environ. Sci. 7 (2010) 211–222, https://doi.org/10.1080/19438151003621334.
[31] P. Sazama, N.K. Sathu, E. Tabor, B. Wichterlová, Š. Sklenák, Z. Sobalík, Structure and critical function of Fe and acid sites in Fe-ZSM-5 in propane oxidative dehydrogenation with N_2O and N_2O decomposition, J. Catal. 299 (2013) 188–203, https://doi.org/10.1016/j.jcat.2012.12.010.
[32] T. Nobukawa, M. Yoshida, S. Kameoka, S.-I. Ito, K. Tomishige, K. Kunimori, In-situ observation of reaction intermediate in the selective catalytic reduction of N_2O with CH_4 over Fe Ion-exchanged BEA zeolite catalyst for the elucidation of its reaction mechanism using FTIR, J. Phys. Chem. B. 108 (2004) 4071–4079, https://doi.org/10.1021/jp030867u.
[33] T. Nobukawa, M. Yoshida, K. Okumura, K. Tomishige, K. Kunimori, Effect of reductants in N_2O reduction over Fe-MFI catalysts, J. Catal. 229 (2005) 374–388, https://doi.org/10.1016/j.jcat.2004.11.009.
[34] M.N. Debbagh, C.S.Md Lecea, J. Pérez-Ramírez, Catalytic reduction of N_2O over steam-activated FeZSM-5 zeolite: Comparison of CH_4, CO, and their mixtures as reductants with or without excess O_2, Appl. Catal. B-Environ. 70 (2007) 335–341, https://doi.org/10.1016/j.apcatb.2005.11.028.
[35] T. Chaki, M. Arai, T. Ebina, M. Shimokawabe, Catalytic reduction of N_2O by various hydrocarbons over Fe-ZSM-5: nature and reactivity of carbonaceous deposits, J. Mol. Catal. A Chem. 227 (2005) 187–196, https://doi.org/10.1016/j.molcata.2004.09.083.
[36] M.A.G. Hevia, J. Pérez-Ramírez, Optimal hydrocarbon selection for catalytic N_2O reduction over iron-containing ZSM-5 zeolite, Environ. Sci. Technol. 42 (2008) 8896–8900, https://doi.org/10.1021/es801971w.
[37] J.A.Z. Pieterse, G.D. Pirngruber, J.A. van Bokhoven, S. Booneveld, Hydrothermal stability of Fe-ZSM-5 and Fe-BEA prepared by wet ion-exchange for N_2O decomposition, Appl. Catal. B-Environ. 71 (2007) 16–22, https://doi.org/10.1016/j.apcatb.2006.08.011.
[38] J. Dedecek, L. Capek, P. Sazama, Z. Sobalik, B. Wichterlova, Control of metal ion species in zeolites by distribution of aluminium in the framework: from structural analysis to performance under real conditions of SCR-NOx and NO, N_2O decomposition, Appl. Catal. A-Gen. 391 (2011) 244–253, https://doi.org/10.1016/j.apcata.2010.06.026.
[39] J. Dedecek, M.J. Lucero, C. Li, F. Gao, P. Klein, M. Urbanova, Z. Tvaruzkova, P. Sazama, S. Sklenak, Complex analysis of the aluminum siting in the framework of silicon-rich zeolites. A case study on ferrierites, J. Phys. Chem. C. 115 (2011) 11056–11064, https://doi.org/10.1021/jp200310b.
[40] P. Sazama, E. Tabor, P. Klein, B. Wichterlova, S. Sklenak, L. Mokrzycki, V. Pashkkova, M. Ogura, J. Dedecek, Al-rich beta zeolites. Distribution of Al atoms in the framework and related protonic and metal-ion species, J. Catal. 333 (2016) 102–114, https://doi.org/10.1016/j.jcat.2015.10.010.
[41] K. Mlekodaj, J. Dedecek, V. Pashkova, E. Tabor, P. Klein, M. Urbanova, R. Karcz, P. Sazama, S.R. Whittleton, H.M. Thomas, A.V. Fishchuk, S. Sklenak, Al organization in the SSZ-13 zeolite. Al distribution and extraframework sites of divalent cations, J. Phys. Chem. C. 123 (2019) 7968–7987, https://doi.org/10.1021/acs.jpcc.8b07343.
[42] L. Benco, T. Bucko, J. Hafner, H. Toulhoat, Periodic DFT calculations of the stability of Al/Si substitutions and extraframework Zn^{2+} cations in mordenite and reaction pathway for the dissociation of H_2 and CH_4, J. Phys. Chem. B 109 (2005) 20361–20369, https://doi.org/10.1021/jp0530597.
[43] M. Boronat, C. Martinez-Sanchez, D. Law, A. Corma, Enzyme-like specificity in zeolites: a unique site position in mordenite for selective carbonylation of methanol and dimethyl ether with CO, J. Am. Chem. Soc. 130 (2008) 16316–16323, https://doi.org/10.1021/ja805607m.
[44] J. Dedecek, B. Wichterlova, Co^{2+} ion siting in pentasil-containing zeolites. I. Co2+ ion sites and their occupation in mordenite. A Vis-NIR diffuse reflectance spectroscopy study, J. Phys. Chem. B 103 (1999) 1462–1476.
[45] L. Drozdova, R. Prins, J. Dedecek, Z. Sobalik, B. Wichterlova, Bonding of Co ions in ZSM-5, ferrierite, and mordenite: An X-ray absorption, UV-Vis, and IR study, J. Phys. Chem. B 106 (2002) 2240–2248, https://doi.org/10.1021/jp0106799.
[46] J. Dědeček, B. Wichterlová, Co^{2+} ion siting in pentasil-containing zeolites. I. Co2+ ion sites and their occupation in mordenite. A Vis−NIR diffuse reflectance spectroscopy study, J. Phys. Chem. B. 103 (1999) 1462–1476, https://doi.org/10.1021/jp9818941.
[47] W.J. Mortier, R.A. Schoonheydt, Surface and solid state chemistry of zeolites, Prog. Solid. State Ch. 16 (1985) 1–125, https://doi.org/10.1016/0079-6786(85)90002-0.
[48] M.C. Campa, I. Luisetto, D. Pietrogiacomi, V. Indovina, The catalytic activity of cobalt-exchanged mordenites for the abatement of NO with CH_4 in the presence of excess O_2, Appl. Catal. B-Environ. 46 (2003) 511–522, https://doi.org/10.1016/j.apcatb.2003.07.003.
[49] V. Indovina, M.C. Campa, D. Pietrogiacomi, Isolated Co^{2+} and $[Co-O-Co]^{2+}$ Species in Na-MOR Exchanged with Cobalt to Various Extents: An FTIR Characterization by CO Adsorption of Oxidized and Prereduced Samples, J. Phys. Chem. C. 112 (2008) 5093–5101, https://doi.org/10.1021/jp711031v.

[50] J. Dedecek, D. Kaucky, B. Wichterlova, Co^{2+} ion siting in pentasil-containing zeolites, part 3. Co^{2+} ion sites and their occupation in ZSM-5: a VIS diffuse reflectance spectroscopy study, Microporous Mesoporous Mater. 35–6 (2000) 483–494, https://doi.org/10.1016/s1387-1811(99)00244-9.
[51] P. Sazama, J. Moravkova, S. Sklenak, A. Vondrova, E. Tabor, G. Sadovska, R. Pilar, Effect of the nuclearity and coordination of Cu and Fe sites in β zeolites on the oxidation of hydrocarbons, ACS Catal. 10 (2020) 3984–4002, https://doi.org/10.1021/acscatal.9b05431.
[52] A. Kornas, E. Tabor, D.K. Wierzbicki, J.E. Olszowka, R. Pilar, J. Dedecek, M. Sliwa, H. Jirglova, S. Sklenak, D. Rutkowska-Zbik, K. Mlekodaj, Activation of molecular oxygen over binuclear iron centers in Al-rich *BEA zeolite, Appl. Catal. B-Environ. 336 (2023), 122915, https://doi.org/10.1016/j.apcatb.2023.122915.
[53] G. Zhao, K. Chodyko, E. Benhelal, A. Adesina, E. Kennedy, M. Stockenhuber, Methane oxidation by N_2O over Fe-FER catalysts prepared by different methods: Nature of active iron species, stability of surface oxygen species and selectivity to products, J. Catal. 400 (2021) 10–19, https://doi.org/10.1016/j.jcat.2021.04.019.
[54] M. Schwidder, M. Santhosh Kumar, A. Brückner, W. Grünert, Active sites for NO reduction over Fe-ZSM-5 catalysts, Chem. Com. (2005) 805–807, https://doi.org/10.1039/b414179b.
[55] A.A. Battiston, J.H. Bitter, D.C. Koningsberger, Reactivity of binuclear Fe complexes in over-exchanged Fe/ZSM5, studied by in situ XAFS spectroscopy 2. Selective catalytic reduction of NO with isobutane, J. Catal. 218 (2003) 163–177, https://doi.org/10.1016/S0021-9517(03)00120-9.
[56] K.I. Hadjiivanov, G.N. Vayssilov, Characterization of oxide surfaces and zeolites by carbon monoxide as an IR probe molecule. Advances in Catalysis, Academic Press, 2002, pp. 307–511.
[57] E. Ivanova, M. Mihaylov, K. Hadjiivanov, V. Blasin-Aubé, O. Marie, A. Plesniar, M. Daturi, Evidencing three distinct FeII sites in Fe–FER zeolites by using CO and NO as complementary IR probes, Appl. Catal. B-Environ. 93 (2010) 325–338, https://doi.org/10.1016/j.apcatb.2009.10.006.
[58] G. Berlier, A. Zecchina, G. Spoto, G. Ricchiardi, S. Bordiga, C. Lamberti, The role of Al in the structure and reactivity of iron centers in Fe-ZSM-5-based catalysts: a statistically based infrared study, J. Catal. 215 (2003) 264–270, https://doi.org/10.1016/S0021-9517(03)00004-6.
[59] V. Blasin-Aubé, O. Marie, J. Saussey, A. Plesniar, M. Daturi, N. Nguyen, C. Hamon, M. Mihaylov, E. Ivanova, K. Hadjiivanov, Iron Nitrosyl Species in Fe-FER: A Complementary Mössbauer and FTIR Spectroscopy Study, J. Phys. Chem. C. 113 (2009) 8387–8393, https://doi.org/10.1021/jp900699m.
[60] M. Mihaylov, E. Ivanova, N. Drenchev, K. Hadjiivanov, Coordination Chemistry of Fe2+ Ions in Fe,H-ZSM-5 Zeolite as Revealed by the IR Spectra of Adsorbed CO and NO, J. Phys. Chem. C. 114 (2010) 1004–1014, https://doi.org/10.1021/jp906213a.
[61] M. Kantcheva, E.Z. Ciftlikli, FTIR Spectroscopic characterization of NOx species adsorbed on ZrO_2 and ZrO_2–SO_4^{2-}, J. Phys. Chem. B 106 (2002) 3941–3949, https://doi.org/10.1021/jp013593o.
[62] A. Zecchina, S. Bordiga, M. Salvalaggio, G. Spoto, D. Scarano, C. Lamberti, Formation of Nonplanar $CuI(CO)_3$Tricarbonyls on CuI–ZSM-5:an FTIR Study at 80 K, J. Catal. 173 (1998) 540–542, https://doi.org/10.1006/jcat.1997.1928.
[63] M. Rivallan, G. Ricchiardi, S. Bordiga, A. Zecchina, Adsorption and reactivity of nitrogen oxides (NO_2, NO, N_2O) on Fe–zeolites, J. Catal. 264 (2009) 104–116, https://doi.org/10.1016/j.jcat.2009.03.012.
[64] L. Benco, T. Bucko, R. Grybos, J. Hafner, Z. Sobalik, J. Dedecek, S. Sklenak, J. Hrusak, Multiple adsorption of NO on Fe^{2+} cations in the α- and β-positions of ferrierite: an experimental and density functional study, J. Phys. Chem. C 111 (2007) 9393–9402, https://doi.org/10.1021/jp0724018.
[65] L. Benco, T. Bucko, R. Grybos, J. Hafner, Z. Sobalik, J. Dedecek, J. Hrusak, Adsorption of NO in Fe^{2+}-exchanged ferrierite. A density functional theory study, J. Phys. Chem. C 111 (2007) 586–595, https://doi.org/10.1021/jp065618v.
[66] I. Malpartida, E. Ivanova, M. Mihaylov, K. Hadjiivanov, V. Blasin-Aubé, O. Marie, M. Daturi, CO and NO adsorption for the IR characterization of Fe^{2+} cations in ferrierite: an efficient catalyst for NOx SCR with NH_3 as studied by operando IR spectroscopy, Catal. Today 149 (2010) 295–303, https://doi.org/10.1016/j.cattod.2009.09.015.
[67] S. Bordiga, R. Buzzoni, F. Geobaldo, C. Lamberti, E. Giamello, A. Zecchina, G. Leofanti, G. Petrini, G. Tozzola, G. Vlaic, Structure and reactivity of framework and extraframework iron in Fe-silicalite as investigated by spectroscopic and physicochemical methods, J. Catal. 158 (1996) 486–501, https://doi.org/10.1006/jcat.1996.0048.
[68] J. Pérez-Ramírez, G. Mul, F. Kapteijn, J.A. Moulijn, Elucidation of the surprising role of NO in N_2O decomposition over FeZSM-5, Kinet. Catal. 44 (2003) 639–647, https://doi.org/10.1023/a:1026189905517.
[69] J. Pérez-Ramírez, F. Kapteijn, K. Schöffel, J.A. Moulijn, Formation and control of N2O in nitric acid production: Where do we stand today? Appl. Catal. B-Environ. 44 (2003) 117–151, https://doi.org/10.1016/S0926-3373(03)00026-2.
[70] B.E.R. Snyder, P. Vanelderen, M.L. Bols, S.D. Hallaert, L.H. Bottger, L. Ungur, K. Pierloot, R.A. Schoonheydt, B.F. Sels, E.I. Solomon, The active site of low-temperature methane hydroxylation in iron-containing zeolites, Nature 536 (2016) 317–321, https://doi.org/10.1038/nature19059.
[71] G. Busca, A.S. Elmi, P. Forzatti, Mechanism of selective methanol oxidation over vanadium oxide-titanium oxide catalysts: a FT-IR and flow reactor study, J. Phys. Chem. 91 (1987) 5263–5269, https://doi.org/10.1021/j100304a026.
[72] C.-T. Wang, R.J. Willey, Mechanistic aspects of methanol partial oxidation over supported iron oxide aerogels, J. Catal. 202 (2001) 211–219, https://doi.org/10.1006/jcat.2001.3288.
[73] R. Kefirov, E. Ivanova, K. Hadjiivanov, S. Dzwigaj, M. Che, FTIR characterization of Fe^{3+}–OH groups in Fe–H–BEA zeolite: interaction with CO and NO, Catal. Lett. 125 (2008) 209, https://doi.org/10.1007/s10562-008-9577-3.
[74] S. Kameoka, T. Nobukawa, S.-i Tanaka, S.-i Ito, K. Tomishige, K. Kunimori, Reaction between N_2O and CH_4 over Fe ion-exchanged BEA zeolite catalyst: a possible role of nascent oxygen transients from N_2O, Phys. Chem. Chem. Phys. 5 (2003) 3328–3333, https://doi.org/10.1039/b300562n.
[75] N.S. Nesterenko, F. Thibault-Starzyk, V. Montouillout, V.V. Yuschenko, C. Fernandez, J.P. Gilson, F. Fajula, I.I. Ivanova, Accessibility of the acid sites in dealuminated small-port mordenites studied by FTIR of co-adsorbed alkylpyridines and CO, Microporous Mesoporous Mater. 71 (2004) 157–166, https://doi.org/10.1016/j.micromeso.2004.03.028.
[76] G. Busca, V. Lorenzelli, Infrared spectroscopic identification of species arising from reactive adsorption of carbon oxides on metal oxide surfaces, Mater. Chem. 7 (1982) 89–126, https://doi.org/10.1016/0390-6035(82)90059-1.
[77] E.-M. El-Malki, R.A. van Santen, W.M.H. Sachtler, Active sites in Fe/MFI catalysts for NOx reduction and oscillating N_2O decomposition, J. Catal. 196 (2000) 212–223, https://doi.org/10.1006/jcat.2000.3034.
[78] D.A. Bulushev, P.M. Prechtl, A. Renken, L. Kiwi-Minsker, Water vapor effects in N_2O decomposition over Fe−ZSM-5 catalysts with low iron content, Ind. Eng. Chem. Res. 46 (2007) 4178–4185, https://doi.org/10.1021/ie061134.
[79] M.H. Groothaert, P.J. Smeets, B.F. Sels, P.A. Jacobs, R.A. Schoonheydt, Selective oxidation of methane by the Bis(μ-oxo)dicopper core stabilized on ZSM-5 and mordenite zeolites, J. Am. Chem. Soc. 127 (2005) 1394–1395, https://doi.org/10.1021/ja047158u.
[80] H. Guesmi, D. Berthomieu, L. Kiwi-Minsker, Nitrous oxide decomposition on the binuclear [FeII(μ-O)(μ-OH)FeII] center in Fe-ZSM-5 zeolite, J. Phys. Chem. C 112 (2008) 20319–20328, https://doi.org/10.1021/jp808044r.